Contract Nonr 839(38)
ARPA Order No. 529

Contract DAHC04-69-C-0077
ARPA Order No. 1442

SPECIE CONCENTRATION MEASUREMENTS UTILIZING RAMAN SCATTERING OF A LASER BEAM

by

George F. Widhopf and Samuel Lederman

Distribution of this document is unlimited.

NOVEMBER 1969

POLYTECHNIC INSTITUTE OF BROOKLYN

DEPARTMENT
of
AEROSPACE ENGINEERING
and
APPLIED MECHANICS

PIBAL REPORT NO. 69-46

SPECIE CONCENTRATIONS MEASUREMENTS UTILIZING RAMAN SCATTERING OF A LASER BEAM

by

George F. Widhopf and Samuel Lederman

This research was conducted in part under Contract Nonr 839(38) for PROJECT STRATEGIC TECHNOLOGY, supported by the Advanced Research Projects Agency under Order No. 529 through the Office of Naval Research; and in part under Contract DAHCO4-69-C-0077, monitored by the U.S. Army Research Office and supported under ARPA Order No. 1442.

Polytechnic Institute of Brooklyn

Department

of

Aerospace Engineering and Applied Mechanics

November 1969

PIBAL REPORT NO. 69-46

SPECIE CONCENTRATION MEASUREMENTS UTILIZING RAMAN SCATTERING OF A LASER BEAM*

by

George F. Widhopf** and Samuel Lederman***

Polytechnic Institute of Brooklyn
Farmingdale, New York U.S. A.

ABSTRACT

The feasibility of utilizing Raman scattering as a diagnostic technique to measure individual specie concentrations in typical gas mixtures found in gas dynamic applications has been investigated and demonstrated. Utilizing this technique, either the local density of a pure gas or the concentration of individual diatomic (or polyatomic) species in a gas mixture can be uniquely determined.

The range and limitations of this technique were investigated and evaluated under controlled static conditions. A Q-switched ruby laser, which has a pulse duration of approximately 10 nanoseconds, was used as a radiation source. The scattered radiation was monitored utilizing a high gain, wide spectral range photomultiplier tube in conjunction with a spectrograph. Measurements were also made utilizing narrow bandpass filters in place of the spectrograph. The species which were investigated include O_2, N_2, CO_2 and CH_4. Quantitative

*This research was conducted in part under Contract Nonr 839(38) for PROJECT STRATEGIC TECHNOLOGY, supported by the Advanced Research Projects Agency under Order No. 529 through the Office of Naval Research and in part under Contract DAHCO4-69-C-0077, monitored by the U.S. Army Research Office and supported under ARPA Order No. 1442.

**Research Associate.

***Associate Professor of Aerospace Engineering.

results are given for these gases in their pure state as well as in various mixture proportions.

It was determined that, with the present experimental configuration, the density of a pure gas or the concentration of a particular specie in a mixture can be determined with good accuracy over a density range of approximately two and one-half orders of magnitude. The lower range for most of the species is a few torr. This capability is independent of the presence of any suspended dust particles in the gas mixture.

The relative and absolute intensity of the scattered radiation from the species investigated were compared with that predicted by theory. Good agreement was obtained. Measurements were also made of the vibrational temperatures of O_2. Fair agreement was obtained for the spectrograph measurements and very good agreement was obtained for those made utilizing the narrow bandpass filters.

A description of the pertinent theory and concepts of Raman scattering is also included as well as a discussion of the limitations of the technique.

TABLE OF CONTENTS

LIST OF TABLES

LIST OF FIGURES

LIST OF SYMBOLS

A	complex amplitude of the incident electric field
B_e	equilibrium rotational constant (vibrationaless state)
B_v	mean rotational constant in a vibrational state; defined by eq. A4-2
$b_{J'K'}^{JK}$	intensity factor of rotational Raman lines
c	velocity of light, $2.99793(10)^{10}$ cm/sec
D_e, D_v	defined by eq. A4-3
E	molecular energy
$\underline{E}$	electric field vector
E_{kn}	defined by eq. A1-23
g_J	probability factor of the rotational state J
h	Planck's constant $6.62517(10)^{-27}$ ergs sec
H^o	Hamiltonian operator
I	intensity
J	rotational quantum number=0,1,2.....
k	Boltzmann constant, $1.38044(10)^{-16}$ erg/^oK
m	molecular mass
$\underline{M}$	induced dipole moment
n_{TP}	index of refraction of air at a given temperature and pressure
N	number of molecular scatterers
O	symbol for O-branch of vibrational-rotational spectral band, where $\Delta J=-2$
P	pressure
$\underline{P}$	dipie moment (polarizability theory)

$[\underline{P}]_{kn}$	induced dipole moment, time dependent
$[P^o]_{kn}$	induced dipole moment amplitude
$\|P_{kn}\|$	transition amplitude
Q	symbol for Q-branch of rotational-vibrational spectral band, where $\Delta J=0$
r	internuclear distance
S	symbol for S-branch of vibrational-rotational spectral band, where $\Delta J=+2$
t	time
T	term value=E/hc, temperature
v	vibrational quantum number=0, 1, 2....
V	potential energy
x, y, z	coordinates fixed in the molecule
X, Y, Z	coordinates fixed in space
Z_J	rotational partition function
$\hat{\alpha}$	polarizability tensor
α'	spherical (isotropic) part of the change of the polarizability
γ'	anisotropic part of the change of the polarizability
r_j	distance of the charges from the center of the molecule
θ	observation angle with respect to the incident radiation (see Fig. 2)
λ	wavelength
μ	reduced mass of molecule

ν	wave number
ρ	depolarization ratio; defined by Eq. (A3-7)
χ	amount of anisotropic scattering in the Q-branch; defined by Eq. (A2-25)
$\dot{\psi}$	wave function amplitude
Ψ	time dependent wave function
ω_e	vibrational frequency

Subscripts

e	equilibrium value (completely vibrationless state); also electronic state
i, j, k	unit vectors in x, y, z and X, Y, Z directions
k, m, n, r	various energy states of the molecule
o	incident value
r	rotational state
v	vibrational state

Superscripts

o	unperturbed state
'	perturbed state

I INTRODUCTION

The development of techniques capable of directly measuring local values of gas density has received much attention in recent years. This capability greatly enhances the information which can be experimentally obtained about gas dynamic flow fields, and could be of particular importance in situations where the determination of specie concentration or local density distributions are important. This is especially true when standard probe techniques interfere with the flow field, or where the relative concentrations of the species being measured are altered by the sampling technique utilized.

Some techniques recently investigated included, electron beam fluorescence,[1-3] Rayleigh scattering[4], and Thompson scattering[5,6]. Each has its own particular use and limitations. The electron beam has an operation upper limit of a few Torr, due to the quenching of the excited molecules through collisions before they are able to emit their radiation. Since the frequency of the emitted light is unique to each molecule, individual species contained in a gas mixture can be determined through a spectrum analysis of the emitted light. The ability to measure the concentration of an individual specie is, however, dependent upon the type and amount of the other components comprising the mixture under consideration, since they determine the degree of quenching present under given conditions.

Thompson scattering, on the other hand, utilizes the scattering of radiation from free electrons in a plasma and therefore, can only effectively measure the electron concentration in a relatively high density "hot" plasma. The technique of Rayleigh scattering involves the

elastic scattering of the incident radiation by the gas molecules themselves. The intensity of this scattered radiation can be directly related to the local gas density of the particular specie under consideration. Since the scattered radiation is of the same frequency as the incident radiation, the source of the scattered radiation can sometimes be indeterminable. That is, any dust which is present, as well as equipment, will also scatter the incident radiation and this may overwhelm the portion scattered by the molecules themselves. While it is true that the scattering cross-section is different for each specie, there is no way to distinguish the identity of each individual specie in the mixture or the amount it contributed toward the total intensity measured, since all scattered radiation is of the same frequency. Therefore, only some "average" density of the gas mixture can be deduced from the Rayleigh intensity measurements.

Obviously, there exists a need for a diagnostic technique which can complement the above techniques and possibly eliminate some of their inherent limitations. The investigation of such a technique is the subject of this paper.

When a beam of monocromatic light traverses a gas mixture, the resultant scattering phenomenon involves both the elastic and inelastic interactions of the photons with the gas molecules. The elastic interaction results in Rayleigh scattering, while that due to the inelastic interaction results in Raman scattering. The Raman scattered radiation consists of radiation whose energy, and therefore, frequency has been changed by an amount characteristic of the energy differences between the stationary energy states of molecules it

encounters. The shift can result in an increa · in energy, and subsequent increase in frequency (Anti-Stokes Line), or a decrease in energy, and subsequent decrease in frequency (Stokes Line), of the scattered radiation. This frequency shift is a unique characteristic of the scattering molecules and is independent of the frequency of the incident radiation. Therefore, the individual species present in the gas mixture can be uniquely distinguished by monitoring the frequencies of the scattered radiation. Not only can one distinguish between the different species comprising a gas mixture, but, by measuring the intensity of each component of the scattered light one can determine, in theory, the individual rotational and vibrational temperature and concentration of each diatomic or polyatomic species in the mixture.

Since the Raman effect is a scattering phenomenon, the only effect of the other species present in the mixture should be the attenuation (due to absorption or re-scattering) of the resulting scattered radiation. Thus, the ability to detect and measure the concentration of a particular species in a mixture, should not be affected by the type or amount of other species present, provided proper precautions are taken in order to attenuate all other wavelengths present. This, of course, assumes that the subsequent attenuation due to the presence of other molecules is negligible (See Section IV). In the same manner, the presence of any dust particles will not affect these results, since the scattering from any dust particles is of the Rayleigh type or has its own characteristic frequency shift.

Raman scattering has been an important tool of chemical physics for nearly half a century.[7-17] Its application was mainly limited to fundamental research investigating the phenomena itself[7-12] and the determination of certain important molecular constants and characteristics

from the resulting spectra.[13-17] In these investigations[13-17], the gas properties, such as density and temperature, were assumed to be known and the scattered radiation was analyzed for the desired information.

It is the intent of this investigation to use the scattered radiation as a diagnostic tool in order to identify unknown species in a gas mixture, as well as to measure their concentration and vibrational temperature. This type of application has been previously proposed and described in the combined effort included in Refs. 18-20, wherein some exploratory experimental measurements were initiated. Raman scattering has also been proposed and used for probing the upper atmosphere.[21]

As described above, Raman scattering, in theory, presents many inviting features. The investigation of the quantitative experimental feasibility of these features and the extent to which they can be used in practice and applied in the realm of gas dynamic measurements is to be explored, herein. To achieve this end, a static calibration under controlled conditions was initiated. An explanation of the theory involved and a discussion of the necessary equations and concepts needed for Raman diagnostics in gas dynamic applications is presented, together with quantitative experimental results. Its applicability and use under varying conditions, as far as gas density, discrimination ability in various gas mixtures, and loss factors will be discussed and determined.

II THEORY

Consider a photon of arbitrary energy $h\nu_o$, which interacts with a molecule in one of its various stationary states characterized by a discrete energy level E. During the interaction between the molecule and the photon, the molecule undergoes a double transition, by first absorbing and then emitting a photon. During the absorption, the energy of the molecule is raised to $E + h\nu_o$, which may or may not be one of its stationary energy states. If this state does not correspond to a stationary state, the photon is scattered in some direction and the molecule falls to a lower energy level. If the molecule returns to its original state E, the energy and frequency of the scattered photon remains unchanged while its direction may be changed. This type of scattering corresponds to the above mentioned Rayleigh scattering. It is possible that the molecule does not return to its original unperturbed energy state E, but changes to a different energy level E_1. This will result in a corresponding change in the scattered photon energy. If $E_1 > E$, the energy of the photon is decreased to $h\nu_o - (E_1 - E)$, while the internal energy of the molecule has been increased by $(E_1 - E)$. If $E_1 < E$, the energy of the photon is increased to $h\nu_o + (E_1 - E)$ and the molecule's internal energy is decreased by $(E_1 - E)$. This latter process can only occur if E is not the ground state energy. Some of the scattered radiation is, therefore, of a different frequency than the incident radiation and is known as Raman scattering. The former process gives rise to what is usually termed the Stokes component, while the latter is termed the Anti-Stokes component of the Raman scattering. These changes are shown diagramatically in Fig. 1.

Now, if the raised energy state of the molecule corresponds to a stationary state, the photon is absorbed. After a finite period of time (corresponding to the mean life of the raised state, which is inversely proportional to the transition probability), the molecule will fall to some lower energy level (original level or any other) E_2, emitting a photon whose energy is equal to $E-E_2$. This process is known as fluorescence and results in radiation of the different frequency than the incident frequency, as does Raman scattering. It differs from Raman scattering, though, in a very fundamental way. That is, fluorescence can only occur for very selected incident light frequencies while Raman scattering can occur for all incident frequencies. The time scale for the respective phenomena to occur is also different. Raman scattering occurs in approximately 10^{-14} seconds,[22] while a nominal mean life for fluorescence to occur is on the order of 10^{-7} seconds.[3]

At any given temperature the molecules in a small volume are distributed over their possible energy states. In thermal equilibrium they are distribured according to the familiar Boltzmann distribution. Therefore, there will always be some molecules in an energy state above the ground state. With this in mind, and remembering that each of the transitions described above have a finite probability of occurring, it is evident that during any scattering process, Raman Stokes and Anti-Stokes as well as Rayleigh components should be expected to occur simultaneously. The intensity of each of these components will, of course, be different.

The intensity of these scattered radiation components can be determined utilizing the perturbation theory of wave mechanics. That

is, a molecular system can be assumed to be perturbed by the incident radiation and the transition probability of this process calculated. (See Appendix I). This procedure determines the intensity of the scattered radiation in terms of a summation over all the possible energy states, (electronic, vibrational, rotational) of the molecule.[7,8,10] The formulation and result is quite complicated and can only be uniquely evaluated in some very restricted cases. Fortunately, Placzek[8] devised a theory which, under certain conditions, eliminated the need of this summation. He introduced the concept of the polarizability, (See Appendix II). Here the sum over the ground states wave functions can be replaced by the polarizability of the molecule with fixed nuclei, and by the effect of the nuclear motions on the polarizability. That is, when a photon interacts with a molecule, the oscillating electric field of the incident radiation induces a dipole moment $\underline{P}$ in the molecule, of magnitude

$$|\underline{P}| = \hat{\alpha}|\underline{E}| \qquad (1)$$

where $\hat{\alpha}$ is the polarizability tensor. This representation is useful, since the components of $\hat{\alpha}$ can be determined experimentally and $\hat{\alpha}$ does, in effect, replace the summation over all the energy states of the molecule, (See Appendix II).

The intensity of scattered light as a function of the polarizability can, therefore, be derived using the usual concepts of wave mechanics. That is, one can formulate the transition probability of the transition under consideration, the square of which is directly proportional to the intensity of the resulting radiation. For a volume of N arbitrarily

oriented molecules this results in

$$I_{S,A} = C_1(\nu_o \pm \nu_{kn})^4 N |P_{kn}|^2 \qquad (2)$$

where $I_{S,A}$ are the Stokes and Anti-Stokes intensities respectively, Watts

ν_o is the wave number of the incident radiation, cm^{-1}

ν_{kn} is the wave number of the Raman shift, cm^{-1}

N is the total number of molecular scatterers

P_{kn} is the transition probability amplitude (See Appendix I-III)

The transition probability amplitude is, in general, a function of the observation angle, the mode of polarization of the incident radiation as well as the specific type of transition under consideration. The vibrational and/or rotational transitions will be considered herein, since in practice almost all Raman spectra recorded results from these types of molecular transitions. The transition probability amplitude for the vibrational-rotational transition as a function of observation angle, for linearly polarized and unpolarized incident radiation is given in Appendix III. Also, included in this appendix is the ratio of the perpendicular to parallel components of the scattered radiation as a function of the observation angle and the incident radiation polarization.

In the experiments described herein, the incident radiation was vertically polarized (See Fig. 2) and the entire vibrational-rotational Raman band was observed. Under these conditions, the intensity of the scattered radiation for an individual specie can be written in the following form (See Appendix II and III)

$$I_{S,A} = C_2 \frac{(\nu_o \pm \nu)^4}{w_e} N \frac{h}{8\pi^2 c\mu} I_o \left[\alpha'^2 + \frac{7}{45}\gamma'^2\chi\right]\Omega \qquad (3)$$

where ν is the wavenumber of the vibrational Raman shift, cm^{-1}

ω_e is the frequency of vibration in cm^{-1}

h is Planck's constant

μ is the reduced mass of the molecule

c is the velocity of light

I_o is the intensity of incident radiation ,Watts

Ω is the solid angle of the observation system

χ is the amount of anisotropic scattering in the Q-branch

(See the Appendices for a discussion of the Q-branch and χ)

C_2 is a constant

α' is the isotropic part of the change of the polarizability

γ' is the anisotropic part of the change of the polarizability

Both α' and γ' are molecular invariants related to $\hat{\alpha}$ as given in Eq. (A2-18,19) in Appendix II. For linear symmetric molecules (XY_2) and tetrahedral molecules (XY_4) the constant μ, in the above formula, is 2m and 4m respectively, where m is the mass of the Y atom.[16]

It is seen from Eq. (3) that the intensity is dependent upon the number of scattering molecules, the frequency of the scattered radiation, the incident intensity, and certain molecular constants.

The determination of the wavelengths of the various Raman components should be done with the greatest degree of accuracy (i.e., better than the resolution required in the investigation). This can be accomplished, for diatomic molecules, by utilizing the vibrating rotator molecular model as described in Ref. (23). The procedure, equations and molecular constants necessary for such a calculation are described and given in Appendix IV.

Utilizing these models the wavenumbers, in vacuo, of the Stokes and Anti-Stokes components can be computed for each species. Since the measurements are usually made in air, the index of refraction of air must be taken into account. The wavelengths of the components can be calculated using the relation $\lambda = 1/\nu n$, where the index of refraction of air (n) as a function of freuqency, temperature, and pressure is given in Appendix V. The Raman wavelengths of some interesting species calculated utilizing the procedure outlined in Appendix IV and V, are shown in Figure 3. Included therein, are the wavelengths for the CO_2 and CH_4 Raman components as computed using the Raman shifts reported in Ref. 15.

The molecular invariants α' and γ', for a given species, should also be known. These invariants, as previously explained, can be determined experimentally. Their exact measurement is a delicate and difficult task and many attempts have been made in the past to determine these constants.[14-17] Examining the available data for α' and γ', it was found that the work in Ref. 15 was very reliable. These results are expected to be accurate within the experimental error of this investigation. The data from other previous investigations are outlined in Table I, together with that used herein, in order to give a better perspective of the type of data available. Certain quantities needed for our calculations, which were derived from the data of Ref. 15, are included in this table. It should be noted that in these investigations, most of the measurements were made of the Q-branch and not of the entire vibrational-rotational band.

Since the intensity of the scattered radiation depends upon the

number of molecular scatterers present in the volume being investigated a measurement of the intensity will give N or the concentration of the particular species under consideration. For any given situation both the Stokes and Anti-Stokes components should be present, therefore, theoretically, the intensity of either component could be used to determine the concentration of a particular specie. In practice, however, the Stokes line should be used, since it is usually more intense at the lower temperatures. Considering only the Stokes components of the Raman scattered radiation, equation (3) can be rewritten, including the attenuation factors introduced by the experimental apparatus, in the form

$$\frac{I_{s_p}}{I_o} = C_2 V N \omega(T) \frac{(\nu_o - \nu)^4}{\omega_e} \frac{h}{8\pi^2 c\mu} [\alpha'^2 + \frac{7}{45}\gamma'^2\chi] \frac{A_l}{r^2} \frac{A_s}{A_i} L \quad (4)$$

where I_{s_p} is the intensity of the scattered radiation from an individual specie as seen by the phototube.

V is the scattering volume, cm^3

N is the concentration of molecular scatterers, particles/cm^3

$\omega(T)$ is the number of molecules in the ground state at the temperature T

A_l is the collecting lens area, cm^2

r is the distance between the scattering center and the collecting lens, cm

A_s is the illuminated area of the slit, cm^2

A_i is the area of the image of the scattering volume on the spectrograph slit, cm^2

L is the transmission factor of all the optics (lenses, filters, grating, etc.) in the system

Equation (4) gives the functional dependence of the scattered intensity upon the various governing independent parameters. It is important to note the linear dependence with number density. Theoretically, a measurement of I_o and I_{s_p}, knowing all other quantities, will yield the number density of the species under consideration.

Taking the ratio of the intensities of the Stokes and Anti-Stokes components, and utilizing the Boltzmann distribution to determine the number of molecules in each vibrational state, results in

$$\frac{I_S}{I_A} = \frac{(\nu_o - \nu)^4}{(\nu_o + \nu)^4} \exp\left[ch\nu/kT\right] \qquad (5)$$

where I_S and I_A are the intensities of the Q-branch. This intensity ratio as a function of temperature is shown in Figure (4) for a few species of interest.

Since the frequency shifts have been determined previously, a measurement of I_A and I_S will determine the vibrational temperature when substituted in Eq. (5). The sensitivity of the determination of vibrational temperature, due to inaccurate measurements of I_S and I_A, is shown for a typical species, in Fig. (5). It must be remembered that the utilization of the Boltzmann relation assumes thermal equilibrium, an assumption which may be violated in some applications.

As seen in Eq. (4) and Table I, the Raman cross-sections are very small and therefore, in relatively short duration measurements, a high intensity source is needed to produce scattered light of sufficient intensity which can be recorded above the local background and instrument "noise". The use of a Q-switched ruby laser (10 nanoseconds

pulse duration) satisfies this requirement and in addition permits the application of this technique in a dynamic situation.

III EXPERIMENTAL FACILITY

The system characteristics given prime consideration in the design of the experimental facility were: safety, elimination of unwanted reflections, and system versatility. Since direct observation (or even indirect viewing after many diffuse reflections) of the laser radiation is dangerous, prime importance was placed on safety. The system (see fig. 6), was therefore, designed so that the laser radiation would be completely enclosed (where possible) in order to avoid any accidents. These enclosures did not interfere with the experimental measurements and were designed for quick adjustment and removal.

As stated previously, the intensity of the Raman components of the scattered radiation is low. Therefore, care must be taken in both its detection and measurement. Since the intensity of the scattered radiation is, in general, a function of the angle between the incident radiation and the viewing system, reflections of scattered radiation into the viewing system must be avoided. This is particularly true if local measurements are to be made. The above statements are applicable for the Rayleigh components as well. therefore, their reflections should also be eliminated. This is especially important, since the intensity of the Rayleigh component is normally at least three orders of magnitude larger than the Raman component, and must be filtered out in order to avoid masking the Raman component. Thus, the additional Rayleigh intensity resulting from reflections can only magnify this problem.

To accomplish this, a radiation absorption chamber (see Fig. 6) was constructed and placed in line with the incident radiation direction. This provided a terminal for the incident radiation, wherein all radiation is internally reflected and absorbed within the chamber, and thus

eliminates the possibility of any reflections into the scattering chamber. A second chamber provided a good background for the viewing system, thus eliminating scattered radiation reflections in line with the viewing system.

Since one of the intentions of the investigation was to find the operational lower limit of the technique, the system had to have vacuum capabilities. Optical paint could, therefore, not be utilized to coat the inner surface in order to avoid reflections, due to its outgasing properties. Therefore, the inner surfaces were black anodized. The inside of the scattering chamber was roughened as well, in order to eliminate the internal reflections more effectively.

The absorption chambers were designed similar to those utilized in Ref. 5, since they were easy to construct and proved very successful, in that investiagtion, in eliminating unwanted reflections. The chambers consisted of black anodized aluminum cones, whose surfaces were degreased, rough buffed, and placed in black anodized aluminum cylinders. The opening to the incident radiation absorption chamber was made large enough to accept the entire beam and yet, only be large enough to allow the chamber to operate effectively. The opening for the background chamber was made to match the viewing system opening. This type of background absorber was chosen, since it seemed to be more reliable than simply depending upon simple absorption at the wall.

The design of the optical system was such that a variable scattering volume could be investigated by adjusting an iris, placed at the exit of the optical system. The f number of the optical system was designed to closely match that of the spectrograph (f/ 4.5). Two

achromatic lenses (22 cm focal length) were used. They were placed so that the image and object were at the focal points of the corresponding lenses, thus providing an image to object ratio of one to one. This permitted a system in which parallel light was obtained between the two lenses, where filters could be placed without any distortion of their bandpass characteristics.

The vacuum system consists of a water cooled 4" oil diffusion pump, coupled with a mechanical roughing pump. The vacuum system is located at the bottom of the test chamber separated from it by a 4" vacuum slide valve. The chamber can be pumped down to 10^{-4} Torr, as measured with an ionization gauge. This was considered to be low enough so that the system would have a minimal amount of impurities even at very low test pressures.

The chamber was designed to accomodate various pressure sensitive instruments as well as a thermometer used to record the test gas temperature. The absolute pressure measurements were made utilizing a barometric type manometer. The instrument has an accuracy of 0.1 Torr, and a scale which can be corrected for changes in room temperature. A baratron was used for absolute pressure measurements below 20 Torr.

The distance between the laser and the scattering center were chosen in order to somewhat simulate those distances to be encountered if one would use the technique in one of our aerodynamic simulation facilities. This distance was also large enough so that the image of the laser rod was inside the incident radiation absorption chamber Photographic views of the experimental apparatus are shown in Figure 7.

Laser System

The system used in these experiments was a TRG Model 104A Ruby Laser System. It can be operated in either a normal or Q-switched mode. In the Q-switched mode the laser output is one (1) joule, released in a pulse of 10 nanoseconds duration (measured at the halfwidth). This results in a peak pulse output of approximately 100 megawatts, which was the approximate operating level for most of the experiments herein. The laser head is cooled with room temperature air and emits radiation at a wavelength of 6943 $\mathring{A}$, which is linearly polarized in the vertical plane.

The energy output of this system is monitored by a TRG Model 100 Thermopile in conjunction with a calibrated TRG Model 102 energy-meter. The pulse shape is monitored by a TRG 105 B photodiode whose output is displayed on a Tektronix 519 oscilloscope. The photodiode has a S-20 spectral response and utilizes a diffusing disk to distribute the light pulse over the entire photosensitive surface. Since the rise time of the photodiode is 0.2 nanoseconds and the rise time of the oscilloscope is 0.29 nanoseconds, the laser pulse, as recorded by this combination, is not substantially distorted. The respective instruments are connected by a special matching 125 ohm, 5 nsec delay cable in order to prevent any ringing of the photodiode circuit.

The monitoring of the laser probe is accomplished by utilizing two calibrated beamsplitters; one of which reflects a small fraction of the main beam into the other beamsplitter, which in turn reflects and transmits part of this beam into the photodiode and thermopile. Both of these beamsplitters were carefully calibrated utilizing the laser as a

source, and two thermopiles, monitoring simultaneously the reflected and transmitted portions of the beam. The thermopile positions were also interchanged in order to cross check the calibration.

Spectrograph

The spectrograph available for use in these experiments was a WARNER & SWASEY Model M-401 Zoom Spectroradiometer. The effective apperature ratio of this instrument is f/4.5. It utilizes a slit assembly which is adjustable, from a minimum width of 25μ to a maximum of 1000μ. The instrument has a plane grating whose ruled area of 64x64 mm had 1180 groves/mm and is blazed for 7500 Å. The efficiency of this grating is 74% of the blaze wavelength and approximately 60% at 6500 and 8500 Å. It has a ghost intensity of less than 0.002% in the first order to 5461 Å and the resolution using a 25μ slit opening is 1.42 Å at 5000 Å.

A high gain photomultiplier (RCA Model No. C31000F) tube, housed in a light sealed container attached to the spectrograph, was utilized to monitor the exit radiation. This tube has good dark current characteristics and has an anode pulse time of 2 nanoseconds at a bias of 2500 volts. Its spectral response is depicted in Fig. 8. A highly stabilized, filtered power supply was used to drive the tube and the variation of the tube gain, as a function of the voltage applied between the anode and cathode, is shown in Fig. 9. The absolute gain was determined using a carefully calibrated helium-neon laser as a source.

The output of the tube was displayed on a high speed Tektronix 454 oscilloscope and recorded on Polaroid film (10,000 ASA speed).

IV DIAGNOSTIC LIMITATIONS AND SYSTEM ATTENUATIONS

Certain limitations associated with Raman scattering can be outlined briefly. Since the Raman cross-sections are very small, a high intensity source is needed in order to produce scattered light of sufficient intensity which can be recorded above the local background and instrument noise. The use of a Q-switched ruby laser (10 nanoseconds pulse duration, 6943 $\mathring{A}$) satisfies this requirement and in addition, permits the application of this technique in a dynamic situation. Since the scattered intensity varies with the fourth power of the frequency, the use of a source which emits high intensity radiation at a high frequency would be more desirable. This, in conjunction with the fact that the sensitivity of the available photodetectors is much greater in the higher frequency range, would increase the efficiency and range of the technique. Unfortunately, such a high power source is not presently available. The use of a higher power Ruby laser would also increase the intensity of the scattered radiation, thereby, increasing the range of the technique.

The Raman Stokes components of interest lie in the near infrared region of the spectrum, when a Ruby laser is used as the incident radiation source. Unfortunately, in this region the sensitivity of available photomultiplier tubes is not very good, (see Fig. 8). For this reason, the phototube selection for use in this investigation was quite tedious. Several RCA as well as Amperex tubes were investigated. The requirements of high gain, wide spectral characteristics and low "noise" were difficult to meet. It became necessary to compromise as far as gain is concerned, and select the RCA Type C31000F (which

is an experimental model), due to its lower than average "noise" and wider than average spectral characteristics.

Since the intensity of scattered light is directly proportional to the local gas concentration, a lower limit is expected to be set, for a given source intensity, on the measureable gas density. Similar limitations are present in the utilization of the electron beam, wherein an upper limit is also introduced due to collisional quenching. Another consideration is the effect of the surrounding molecules on the scattered light. This will manifest itself in the absorption of photons and the subsequent scattering of these Raman photons by the gas between the scattering center and the detector. Similar absorption and scattering considerations are also true for the light emitted by the excited molecule in the electron beam fluorescence technique before its detection is accomplished.

Subsequent scattering of Raman light will be predominantely of the Rayleigh type due to its large cross-section and therefore, its frequency will be unchanged. The only problem will be that losses will occur since the Raman light is scattered at various angles other than that of the viewing system and therefore, some will be lost before reaching the detector. The amount of the incident radiation which is lost due to scattering before reaching the volume under investigation and the amount of Raman radiation which is re-scattered before being detected are both very small. This can be readily seen by considering the cross-sections involved (either Raman or Rayleigh). The amount lost due to absorption will be a function of specific frequency considered. This should also be very small, except when the frequency of the

scattered radiation corresponds to a strong absorption band of another specie present in the mixture.

The losses and attenuations introduced by the measurement techniques and system design must now be considered. The system losses manifest themselves mainly in the attenuations and reflections of the incident and scattered radiation by the test gas and optics in the system. These losses can be most easily combined in a calibration factor and were determined utilizing a helium-neon laser (6328 Å) and a very sensitive, calibrated thermopile. The radiation emitted by this laser is polarized in the vertical plane as is the ruby laser used herein. The transmission factors through all of the system optics was measured to be 0.608.

The major instrument losses will be encountered due to the spectrograph, which is used to monitor and measure the separate components of scattered radiation. Since each of these instruments has its own inherent characteristics as far as losses are concerned, they must be determined in each individual case. The losses are a function of frequency and therefore, must be known over a range of wavelengths.

In order to minimize these losses, the viewing system optical characteristics should be matched to the particular spectrograph utilized, and the grating should be selected to give the maximum efficiency over the spectral range of interest. The attenuation due to the grating was determined utilizing the data supplied by the manufacturer. The attenuation of any filters which were used in the system was obtained from the transmission curves supplied by the manufacturer. These transmission factors were re-checked utilizing various spectral lamps.

The attenuation of the spectrograph was also checked, utilizing the helium-neon laser and was found to agree with the expected attenuation.

In consideration of the above, one would expect the most severe limitation to be the availability of photodetectors capable of resolving low light intensity levels.

V. EXPERIMENTAL PROCEDURE AND RESULTS

As stated in the introduction, the purpose of this investigation is to determine the feasibility of using Raman scattering as a diagnostic technique in order to determine the specie concentration and vibrational temperature of various gases, both in a pure state and in mixtures. As seen in Eq. (4), the intensity of the Raman components vary linearly with specie concentration. It should, therefore, be determined in what range the intensity of the scattered radiation, as recorded in an actual situation, is linear. This would determine, under these experimental conditions, the range in which a measurement of the scattered intensity from a particular specie would provide data from which its concentration could be calculated. This would also provide a calibration curve for each specie which could be utilized to determine the concentration of individual species in a mixture.

The above was accomplished by filling the chamber with the desired gaseous specie (commerically pure), pulsing the laser, and recording the scattered intensity as a function of gas pressure. The pressure (and therefore the density, since the temperature of the test gas remained at room temperature) was subsequently varied over nearly three orders of magnitude. In all tests the spectrograph was preset at the desired Raman wavelength, and the slit width set at 1000μ. Two filters were placed in the viewing system chamber provided for them. One filter had a narrow reflection band (300 $\mathring{A}$), centered at 6943 $\mathring{A}$, in order to attenuate the Rayleigh component. It passed all other wavelengths at a slight attenuation ($\approx$25%). The second filter has a

100 Å bandpass centered at the desired Raman wavelength and blocked all other wavelengths. This combination provided, in all cases, an attenuation of the Rayleigh component of at least five orders of magnitude, while attenuating the Raman component by approximately 50%. The magnitude of the attenuation of the Rayleigh component which is required in any specific application is dependent upon the ghost ratio of the grating utilized, the individual spectrograph characteristics, and the ratio of the Rayleigh to Raman intensity.

The utilization of these filters eliminated the possibility that any of the other components would mask the desired Raman component, due to their much greater intensity (Rayleigh Ghosts), or that they would be recorded if one of their higher orders (due to the dispersion of the grating) corresponded to the Raman wavelength being measured. This precaution did not, however, eliminate the possibility of recording radiation of the same frequency as the Raman components, which originated from another source; (e.g., if certain wavelengths of the emission spectra of the gas mixture corresponded to some of the Raman wavelengths being observed). In this case, a measurement of the background radiation must be made before any Raman scattering measurements are undertaken and accounted for in the subsequent data reduction. The nonexistence of this background radiation was determined by the subsequent tests described below. The latter considerations are not so important under the present conditions, but, they may be important under conditions where there is some substantial background radiation present.

In each test, the incident laser pulse as well as the scattered

intensity were monitored. Thus, any variation in the laser pulse could be determined and accounted for in the subsequent data reduction. The incident laser pulse was monitored by a thermopile and a photodiode(see Fig. 6 and the description of the equipment). A typical response of the photodiode depicting the incident laser pulse waveshape is shown in Fig. (10a). As stated previously, the response times of the recording equipment was fast enough so that the laser pulse waveshape was not appreciably distorted. The power of the incident laser pulse could, therefore, be determined from the response of the photodiode (using the halfwidth) and the thermopile output.

Typical scattering pulses, as monitored by the phototube in high and low density tests, are shown in Fig. (10b) and Fig. (10c), respectively. One notices the raggedness of the pulse at lower pressures. Since the rise times of the phototube and the oscilloscope are about 2 nsec and the decay time of the phototube is several times longer, the waveshape of the scattered radiation is asymmetrical. This could not be avoided, due to the limited availability of phototubes which could be used in this investigation.

Pure Gases:

This procedure was followed in the testing of pure O_2, N_2, CO_2 and CH_4 gases, the results of which are shown in Figs.(11-18) respectively. The data have been plotted on a overlapped chartesian scale (Figs. 11, 13, 15 and 17) in order to give a better idea of the accuracy of the measurements; and on a log-log scale (Figs. 12,14,16 and 18) in order to give an overall perspective of the range of the data as well as a better idea of the accuracy at the lower pressures.

Included in each figure is the theoretical linear distribution as given by Eq. (4), as well as the characteristic observation dimension D. This dimension, used in conjunction with the beam size, defines the scattering volume observed (refer to the diagram in Fig. (6)). In all the tests described herein, the incident beam diameter (6mm) was kept approximately constant. The results presented in these figures have been nondimensionalized with respect to the intensity of the scattered radiation recorded at a pressure of 760 Torr for each specie. This factor is also included in the legend, together with the corresponding incident laser intensity.

Utilization of the above mentioned slit setting (100μ), allowed the observation of the entire vibrational-rotational Raman Stokes band. In the case of carbon dioxide, which has four Raman Stokes components, the intensity recorded when the spectrograph was utilized, was the combined intensity of the vibrational-rotational bands at 7683 and 7696 Å. A separate measurement was made of the combined intensity of the bands at 7612 and 7623 Å. In this case, the recorded intensity of the scattered radiation was $8.2\,(10)^{-8}$ watts, for an incident radiation intensity of 75 megawatts.

In the case of CH_4, two Raman components exist in the wavelength range of interest. The component which was monitored (8704 Å) is due to a totally symmetric vibration of the molecule and results from an isotropic change in the polarizability. Thus, this component is only a function of α' and has no accompanying rotational lines. The other component (8737 Å) is due to a doubly degenerate vibration and is only a function of γ'. Since a narrow bandpass filter centered at 8704 Å

was not available, measurements of the intensity of the CH_4 Raman component could only be made utilizing the spectrograph. Another reflection filter (6943 $\mathring{A}$) was used in order to assure that the Rayleigh component was sufficiently attenuated.

Good agreement between the measured Raman intensity and theory, over a range of approximately two and one-half orders in magnitude in density, is noticed for all the species. Almost all of the data points fall within 10% of the theoretical line. The accuracy is better at higher pressures and decreases to 15-20% at the lowest pressure. The lower limit for N_2 (10 Torr) is higher than O_2 and CO_2 (3-4 Torr). This is due to the fact that the Raman scattering cross-section of N_2 is smaller than either O_2 or CO_2 and also, because the phototube is less sensitive at this wavelength. The lower efficiency of the grating and the higher attenuation of interference filters at the longer wavelengths, also, contribute to this result. These considerations are, also, the reason why the lower limit of CH_4 is not lower than that of all the other species, even though its scattering cross-section is larger. A major factor in the determination of these lower density limits is the magnitude of the phototube "noise". That is, at pressures below these limits the intensity of the scattered radiation is within the "noise" of the phototube, and therefore, is not measurable.

The choice of limiting the measurements to an upper limit of 760 Torr was purely based on matters of system integrity and convenience. The upper range of the technique can easily be extended to higher pressures; that is, on the order of 2-3 atmospheres (e.g. some measurements made in Ref. 15 and 17 were made at a pressure of 2 atmospheres).

As indicated in the introduction, the upper limit of the electron beam fluorescence technique is a few Torr, due to the quenching of the excited molecules. The data as presented here, indicates that if Raman scattering from O_2 or CO_2 was used as a diagnostic technique, it is possible to measure densities within the upper bounds of the electron beam technique. The Raman scattering technique, therefore, complements as well as presents the possibility of supplementing it, with the use of more sensitive phototubes or higher powered lasers.

Included in these Figures (11-16) are the results of tests conducted without the spectrograph, utilizing only narrow bandpass filters to select the proper Raman wavelength. Here the spectrograph was removed and an iris placed at the image of the scattering volume. In these tests, two narrow reflection band filters, centered at 6943 $\mathring{A}$, were used in conjunction with the individual Raman filters. In all cases this type of filter combination attenuated the Rayleigh component by at least eight orders of magnitude or more.

As in the tests utilizing the spectrograph, measurements were made at very low pressures in order to determine if there was any outside light leakage or background intensity at each wavelength of interest. Tests were also conducted at various pressure levels in order to determine if there was any background radiation present. These tests showed the presence of neither. The transmission of any Rayleigh or other radiation through the spectrograph, or through the narrow bandpass filters, was extensively tested and determined to be of such a low magnitude that they were not measurable. These tests were conducted under the most severe conditions encountered in the experiments

and the filters were found to be more than adequate. Measurements of the Raman scattered intensity were made immediately after filling the chamber as well as after the dust had been allowed to settle. The presence of suspended dust particles was found (within experimental error) not to have any effect on the measurements. As discussed in the introduction this result was expected. Only when the wavelength of the scattered Raman radiation from the dust particles is close (i.e. not within the resolution of the spectrograph) to the Raman wavelength associated with a gaseous specie of interest, will the presence of dust effect the Raman scattering measurements.

In the tests conducted utilizing narrow bandpass filters the diameter of the iris opening was set at approximately 2.5 mm. The crossing of its image with the incident beam defines the scattering volume being observed, as described in Fig. (6). The data is presented in the same manner as was the spectrograph data, where the respective nondimensionalization factor is also included in each figure. It should be noticed that in the case of CO_2, all four of the Raman bands were now observed simultaneously.

Since the attenuation of the narrow bandpass filters was much less than that of the spectrograph, it was possible to achieve better spacial resolution at a given pressure, when the filters were utilized, without any sacrifice of the intensity of the scattered radiation. Thus, the scattering volume observed when the narrow bandpass filters were utilized, was reduced to approximately one-fourth that of the volume which was observed when the spectrograph was utilized. As can be seen from these figures, the accuracy of the measurements utilizing either method

is about the same.

The relative intensities of the Raman components of the different species considered, were checked with that predicted by theory utilizing the experimental values of α' and γ' obtained from the data in Ref. (15 and 16). The comparison was made for the intensities measured using narrow bandpass filters. These results are presented in Table II where very good agreement is noticed. Included therein, are the values of α' and $\chi(\gamma'/\alpha')^2$ used to compute the theoretical value of the scattered intensity. It should be pointed out that, in the case of CO_2, the combined intensity of all the Raman Stokes components was compared to that predicted by theory. It is noticed that intensity measured utilizing the spectrograph is higher than the theoretical value. This probably occurred due to some overlapping of the frequency band resolved when separate measurements of the intensities of 7612, 7623 Å and 7683, 7696 Å bands were made. This did not effect any of the subsequent results, since the spectrograph was always kept at the same wavelength setting when mixtures involving CO_2 were being analyzed.

Due to the wavelength resolution of the spectrograph a portion of the CH_4 Raman band at 8787 Å was measured simultaneously with the component at 8704 Å. Since the theory as presented herein for XY_4 molecules is valid only for the totally symmetric vibration, the theoretical intensity of the CH_4 components including the contribution due to the doubly degenerate vibration could not be readily calculated.

The intensity of the O_2 Raman Stokes component was calculated using Eq. (4) (where C_2 was taken to be $8\pi^4$)[18] and compared to that computed from the scattered radiation trace. The spectrograph

measurement was found to be approximately 17% lower than that predicted by theory, while the intensity measured utilizing narrow bandpass filters was approximately 10% higher. These differences are within the experimental error resulting from the measurement of each attenuation factor, as well as the estimate of the scattering volume. It also must be remembered that the values of γ' and α' used to predict the theoretical intensity are probably only accurate within 10%. Since the relative intensities agree with that predicted by theory, the differences between the calculated and measured intensity are probably due to the estimate of the scattering volume.

It should be mentioned that the same type of tests were performed using Hydrogen as the scattering medium. Unfortunately, due to the very low sensitivity of the phototube at this wavelength, no reliable results could be obtained. An available phototube with an S-1 response was considered, but, while its sensitivity was better at 9764 Å, its gain was less, rendering it less useful than the RCA Type C31000F phototube.

Mixtures:

Figures (11-16) can be considered to be calibration curves and, therefore, be used for the investigation of the feasibility of determining individual specie concentrations in various gas mixtures. As stated in the introduction, the determination of the concentration of an individual specie in a gas mixture should be independent of the type and amount of the other components comprising the mixture. (Here it is understood that the subsequent rescattering or absorption of the scattered photons by the surrounding molecules is assumed to be negligible (see

discussion of limitations)}. Thus, the goal of these measurements is the demonstration, under controlled experimental conditions, of the validity of this diagnostic capability.

In these tests, various gases were mixed in known proportions and the intensity of the various components was recorded. Tests were conducted using a spectrograph and also using narrow bandpass filters in order to select the wavelengths of interest.

Measurements were made in order to determine if there was any response for a particular specie when it was not present in the mixture, and the density of other species was high. In all tests the result was negative, indicating that only the intensity of the specific component of interest was recorded. The same type of check was performed when the narrow bandpass filters were utilized. Here it was found that the CO_2 and O_2 filters each transmitted a very small percentage of the other's component. The amount was measured and used to correct subsequent measurements. This, of course, could be entirely eliminated with the use of filters with a much narrower bandpass.

As stated before, the filters utilized herein sufficiently attenuated the Rayleigh component, even when suspended dust particles were present in the gas mixture. It must be remembered, however, that in the case of a mixture, the Raman components are proportional to the individual specie concentration, whereas the Rayleigh component is proportional to the total mixture density. Therefore, it is the mixture density (plus the presence of dust particles) which must be considered in the determination of the proper Rayleigh attenuation needed in a particular situation.

Initial tests were conducted in two component mixtures (O_2 and N_2) utilizing a spectrograph in order to select the desired wavelength. Here one component was held at a constant partial pressure, while the other was varied over a range of partial pressures. This would show the relative accuracy of individual specie concentration measurements under various mixture proportions. The results of these tests are shown in Fig. (19). The results are plotted according to the mixture considered, where the ordinate is the individual specie partial pressure. Therefore, the total mixture pressure is obtained by selecting a mixture and adding the various partial pressures indicated by the symbols on or near the vertical line emanating from the desired mixture number. The accuracy of these results are seen to be within those encountered in the pure specie tests. In general, it was found to be a good practice to repeat a few calibration measurements each day, in order to eliminate any error due to any subsequent change in the system characteristics.

Other measurements were made involving three component (O_2, N_2, and CO_2) mixtures. These were made utilizing a spectrograph and are presented in Fig. (20). Again, it is seen that each component can be determined with an accuracy equivalent to the pure situation. Mixture number 10 in Fig. (20) shows that species in a three component mixture can be measured with the same degree of accuracy as in the pure tests, even in a mixture where the total mixture pressure is relatively low (60 Torr). Mixture number 11 gives the analagous result for a high mixture pressure case (750 Torr).

Analagous results were found when narrow bandpass filters were utilized, and are shown in Fig. (21). Included herein, are measurements

of very small amounts of trace species in high density gas mixtures. The amount of an individual trace specie ranged fr m approximately 0.4 to 2.5% of the total mixture. (See mixture No. 1 to 8 in Fig. 21). The error encountered increased as the amount of trace specie was decreased, being approximately 10-15% at partial pressures above 10 Torr. This was, of course, expected, since this was also the approximate error encountered in the previous tests using pure gases.

All of these measurements indicate that, in a given situation, if the proper precautions have been taken in order to attenuate all other wavelengths, individual specie concentration measurements (and their range) are independent of the density of the other mixture components and are governed exclusively by their own individual concentrations. The demonstration of this diagnostic feature was the goal of this aspect of this investigation.

It must be remembered, however, that certain species may have absorption bands which may correspond to the Raman wavelength of another species in the mixture. In this case the attenuation of the Raman intensity may be significant and must be considered. The presence of any background radiation, which has components of the same wavelength as the Raman radiation, must also be considered and accounted for. These factors must be investigated in each individual application. However, it should be pointed out that these are limitations common to all optical techniques. The effect of subsequent re-scattering of the Raman photons is always small, due to the small cross-sections involved and can usually be neglected.

Temperature Measurements:

A few tests were conducted in order to determine the feasibility of determining the vibrational temperature of a particular gas by measuring the intensity of the Raman Stokes and Anti-Stokes components as indicated in Eq. (5). As shown in Fig. (4), the ratio of Raman Stokes to Anti-Stokes components are on the order of 10^3 to 10^5, at temperatures corresponding to room temperature. The vibrational temperature could, therefore, only be measured for O_2, at 760 Torr, since here the ratio was small enough, and the signal large enough, to allow the measurement of the intensity Anti-Stokes component. The results are included in Table III. Measurements were made using both a spectrograph and narrow bandpass filters as indicated in the table.

As is noticed in Fig. (5), the sensitivity of the temperature, to the measured intensity ratio, is small at low temperatures, and large at high temperatures. This in some way offsets the fact that the intensities of the various Anti-Stokes components are low at low temperatures and, therefore, are subject to more error due to the limited sensitivity of the available phototubes. The vibrational temperature as measured utilizing a spectrograph (D=6mm) averages 14% higher than the actual temperature of the gas, while the measurements using narrow bandpass filters (D=2.5mm), average to about the correct value. This is probably due to the fact that the intensity recorded using filters is higher, thus, these measurements are less sensitive to the tube "noise" characteristics.

As indicated in Eq. (3), the intensity of the scattered Raman radiation is a function of the temperature of the gas. At low temperatures,

this dependence is weak. In any given situation, the simultaneous measurement of I_S and I_A would provide a measurement of the temperature and the concentration. Thus, a calibration made at a lower temperature could be adjusted through the utilization of Eq. (3) and the measured gas temperature. In this case, a calibration which is made at a low temperature can be used as a convenient means of determining the attenuation of the entire system.

The ratio of the intensity of the Raman Stokes to the Rayleigh component was also measured for each specie and compared to that predicted by theory. For a radiation source which is polarized in the vertical plane this ratio is of the form

$$\frac{I_S}{I_R} = \frac{(\nu_o - \nu)^4}{\nu^4} \frac{h}{8\pi^2 \mu \omega_c} \frac{(45\alpha'^2 + 7\chi\gamma'^2)}{(45\alpha^2 + 7\chi\gamma^2)}$$

The experimentally determined values of α' and γ' described previously were used to predict the Raman Stokes intensity, while the values of α were determined from the refractive indices listed in Ref. (27). The polarizability, α, can be related to the index of refraction of a particular gas in the following manner[16]

$$\alpha = \frac{n-1}{2\pi N}$$

In the calculations described herein, γ was assumed to be negligible. The measured values of I_R included small contributions due to the simultaneous measurement of the pure rotational Raman components whose wavelengths are close to that of the Rayleigh component. The results are included in Table IV where very good agreement is noticed for all species except CO_2. Since the Rayleigh intensity is

appreciably increased when dust is present, these measurements were made after the suspended dust particles were allowed to settle. Measurements of the Rayleigh intensity taken immediately after filling the chamber were often as much as an order of magnitude higher than that measured after the dust had been allowed to settle overnight. The presence of such dust particles probably accounts for the discrepancy in the results as presented for CO_2.

Discussion:

It has been demonstrated that Raman scattering can be used as a diagnostic technique in order to determine individual specie concentrations in gas mixtures. In a given application the specie concentration of a particular gas can be determined either using a calibration curve of the type depicted in Figs. (11-18), or utilizing Eq. (4). The utilization of Eq. (4) is more tedious and less accurate, since it requires the separate measurement of many attenuation factors and depends upon previously measured quantities such as α' and γ'. It also depends upon a measurement of the scattering volume, a measurement which is very inaccurate at best. The equations should, therefore, be looked upon as giving the appropriate functional dependence of the scattered radiation upon the various governing independent parameters. Thus, any variation in the scattered intensity, due to changes in any of the governing parameters can be predicted utilizing this equation.

The results which are presented here are dependent upon the experimental arrangement and equipment utilized. A few ways in which either the spacial resolution or density range can be improved

can be briefly outlined. In some applications, due to the presence of background radiation, better wavelength resolution may be required than that utilized in these experiments. The use of a cylindrical lens, to image the scattering volume on the spectrograph slit, can effectively increase the amount of energy entering the spectrograph, (by decreasing slit attenuation), thus allowing the use of a smaller slit opening. This could be accomplished with the use of a lens system which reduces the image to object ratio. All these factors are subject to other considerations, including any subsequent change in the solid angle of the viewing system. An improvement in the wavelength resolution of the narrow bandpass filters can be accomplished simply by utilizing filters with a very narrow bandpass.

The spacial resolution can be improved by changing the incident beam size and/or the utilization of a smaller observation iris. The beam diameter at the scattering center can be changed by varying the incident optical configuration. Thus, the spacial resolution and the lower density range needed in each application must be considered and balanced in order to determine the proper beam size, iris opening and slit width (or bandpass if filters are used) to be used. Certainly, these factors become more critical at the lower density range. In most applications it would seem to be more practical to use the narrow bandpass filters.

Also, as indicated in the discussion of the attenuation factors, the use of higher gain and lower "noise" phototubes, and higher powered and/or higher frequency laser can also improve the range of the technique.

VI. CONCLUSIONS

In view of the above, it may be stated that a technique has been demonstrated which is capable of:

1. uniquely identifying individual diatomic (or polyatomic) species in a gas mixture.
2. measuring the concentration of a pure gas over a range of several orders of magnitude in density.
3. measuring the concentration of a particular specie in a gas mixture. This measurement is independent of the density of the other components of the mixture.
4. measuring the vibrational temperature in gases where the number of molecules present in the first vibrational excited state is not insignificant.
5. measuring densities (concentrations) at levels comparable to the upper limit of the electron beam.
6. measurements not effect (as in Rayleigh scattering) by the presence of dust particles in the gas.
7. measuring specie concentrations in high velocity flow (due to the shortness of the laser pulse duration).
8. measurement of local values of a stationary or flowing gas without the influence of disturbing probes.

VII REFERENCES

1. Muntz, E.P., "Measurement of Rotational Temperature, Vibrational Temperature, and Molecule Concentration, in Non-Radiating Flow of Low-Density Nitrogen," UTIA Rept. No. 71, 1961.

2. Gadamer, E.O., "Measurement of the Density Distribution in a Rarefied Gas Flow Using the Fluorescence Induced by a Thin Electron Beam," UTIA Rept. No. 85, March 1962.

3. Muntz, E.P. and Marsden, D.J., "Electron Excitation Applied to the Experimental Investigation of Rarefied Gas Flows," in Rarefied Gas Dynamics, Ed. by J.A. Laurmann, Vol. II, 1963, Academic Press.

4. Sadowsky, C.M. and Vanoverschelde, J.E.H., "The Measurement of Mass Density in a Turbulent Wake by Means of Rayleigh Scattering from a Laser Beam," TN 1764/67, Canadian Armament Research and Development Establishment (CARDE), Quebec, Canada.

5. Gerry, E.T. and Rose, D.J., "Plasma Diagnostics by Thompson Scattering of a Laser Beam," Journal of Applied Physics, Vol. 37, No. 7, June 1966, pp. 2715-2724.

6. Patrick, R.M., "Thompson Scattering Measurements of Magnetic Annular Shock Tube Plasmas," Physics of Fluid, Vol. 8, No. 11, Nov. 1965, pp. 1985-1994.

7. Kramers, H.A., and Heisenberg, W., Z. Physik 31, 681 (1925).

8. Placzek, G., "Rayleigh Strenung and Raman Effect," Hanbuch der Radiologie, Leipzig: Akademische Verlagegesellshaft VI, 1934.

9. Bhagavantam, S., Scattering of Light and the Raman Effect, Chemical Publishing Co., 1942.

10. Stoicheff, B.P., "High Resolution Raman Spectroscopy," Advanced in Spectroscopy, Vol. I, INTERSCIENCE, 1959.

11. Mizushima, San-Ichiro, "Raman Effect", Handbuch Der Physik, Vol. XXVI, Light and Matter II, Springer-Verlag, 1958.

12. Herzberg, G., Infrared and Raman Spectra of Diatomic Molecules, D. Van Nostrand Co., Inc., New York, 1945.

13. Wilson, E.B., Decius, J.C., and Gross, P.C., Molecular Vibrations, McGraw-Hill Book Co., 1955.

14. Berstein, H.J., and Allen, G., "Intensity of the Raman Effect, I. Reduction of Observed Intensity to a Standard Intensity Scale for Raman Bands in Liquids," Journal of the Optical Society of America, Vol. 45, No. 4, 237, April 1955.

15. Yoshino, T., and Bernstein, H.J., "Intensity in the Raman Effect, VI The Photoelectrically Recorded Raman Spectra of some Gases," Journal of Molecular Spectroscopy, 2, 213, 1958. Also Personal Communication.

16. Standsbury, E.J., Crawford, M.F., and Welsh, H.L. ," Determination of Rates of Change of Polarizability from Raman and Rayleigh Intensities," Canadian Journ of Physics, 31, 954, 1953.

17. Golden, D.M. and Crawford, B., "Absolute Raman Intensities I. Method for Molecules in the Gas Phase," Journal of Chemical Physics, Vol. 36, No. 6, 1654, 1962.

18. Urtz, R.P., "Plasma Diagnostics Using the Raman Effect," RADC-TDR-64-5, 1964, Rome Air Development Center, Griffiss AFB, N.Y. DDC No. 434-761.

19. Sodha, M.S., Varshni, Y.P., and Daley, J.T., "Spectrographic Detection of Raman Lines; Theory of Plasma Diagnostics Using The Raman Effect," Republic Aviation Corp. Report No. RAC 1195-1, November 1963.

20. Urtz, R.P., "Plasma Specie Probe Techniques," RADC-TR-66-793, 1967.

21. Cooney, J.A., "Measurement on the Raman Component of Laser Atmosphere Backscatter," Applied Physics Letters, Vol. 12, 1968, pp. 40-42.

22. Garlick, G/F.J., "Luminescence," Handbuch Der Physik, Vol. XXVI, Light and Matter II, Springer-Verlag, 1958.

23. Herzberg, G., Spectra of Diatomic Molecules, D. VanNostrand Co., Inc., New York, 1945.

24. Rank, D.H., "The Index of Refraction of Air," Advances in Spectroscopy, Vol. I, Interscience, 1959.

25. Woodward, L.A. and Long, D.A., "Relative Intensities in the Raman Spectra of Some Group IV Tetrahalide," Trans. Faraday Society, 45, 1131, 1949.

26. Pauling, L. and Wilson, E.B., Introduction to Quantum Mechanics, McGraw-Hill, 1935.

27. Landolt-Bornstein, Zahelnwerte und Funktionen . 6 Auflage, II Band, 8 Teil, 1962.

VIII APPENDICES

The following Appendices present a short summary of some of the basic theory of the Raman effect. Most of the information contained herein is available in various references [7-13], and the following presentation follows the derivations presented in these references to some degree. Each of the above references presents the information and derivation suited and limited to its own needs and scope of applicability. Also, much of the information contained therein pertains to applications and substances not of interest in gas dynamic applications.

It is the intent of these Appendices to present the desired quantum theory necessary for the understanding and use of the Raman effect for gas dynamic applications, in a readily available place and in a somewhat complete form. An attempt has been made to include only the necessary details needed for the understanding of the Raman effect and to include the generality needed for various gas dynamic applications. These Appendices will, hopefully, illucidate the theoretical description presented in the main text and eliminate the initial necessity of excessive referral to the references.

For more detailed information, the references indicated above should be consulted, together with the other references listed in the bibliography.

APPENDIX I

QUANTUM THEORY OF RAMAN SCATTERING

The quantum mechanical derivation of the scattered intensity using the perturbation theory of wave mechanics, first derived in Reference 7, will be presented herein. This presentation follows somewhat that contained in References 7, 8, and 11, and is included herein for completeness. The more lucid portions of each derivation have been followed in order to obtain, in the author's opinion, a clear description of the pertinent aspects of the theory.

The time dependent Schrodinger wave equation can be written in the form

$$H^{o}\Psi^{o} = \frac{-h}{2\pi i}\frac{\partial \Psi^{o}}{\partial t} \qquad \text{(A1-1)}$$

where Ψ^{o} is the time dependent wave function and H^{o} is the quantum mechanical Hamiltonian operator which is given in chartesian coordinates by

$$H^{o} = \frac{-h^{2}}{8\pi^{2}} \sum_{\alpha} \frac{1}{m_{\alpha}} \left\{ \frac{\partial^{2}}{\partial x_{\alpha}^{2}} + \frac{\partial^{2}}{\partial y_{\alpha}^{2}} + \frac{\partial^{2}}{\partial z_{\alpha}^{2}} \right\} + V \qquad \text{(A1-2)}$$

where V is the potential energy of the system and α indicates a specific particle.

The solution for a molecule in the state k is of the form

$$\Psi^{o}_{k} = \psi_{k} \exp\left[\frac{-2\pi i}{h} E_{k} t\right] \qquad \text{(A1-3)}$$

where E_{k} is the molecular energy in the k state and ψ_{k} is the time independent wave function amplitude.

If a light wave of frequency ν_{o} (where ν_{o} does not correspond to an absorption frequency of the molecule), and of wavelength large in

comparison to the molecular dimensions falls on a molecule, its energy will be changed by the oscillating electric field E of the incident light. The amount of this energy change will be equal to - EM, where $M=\sum_j e\eta_j$ is the electric moment of the molecule. Therefore, to a first approximation the interaction can be described as the inducement of a dipole moment in the molecule.

The incident electric field, E, can be described by

$$\underline{E}= \underline{A} \exp [-2\pi i\nu_o t] + \underline{A}^* \exp [2\pi i\nu_o t] \qquad \text{(A1-4)}$$

where $\underline{A}$ is a complex vector and $\underline{A}^*$ is its complex conjugate. Therefore, the governing Schrodinger wave equation for the perturbed molecular system can be written as

$$(H^o - \underline{M}\,\underline{E})\Psi = \frac{-h}{2\pi i}\,\frac{\partial \Psi}{\partial t} \qquad \text{(A1-5)}$$

where Ψ is the wave function of the perturbed system. If the molecule is in the state k before the interaction, then the wave function of the molecule after irradiation can be written in the form

$$\Psi = \Psi_k^o + \Psi_k' \qquad \text{(A1-6)}$$

Substituting this form of the wave function for the perturbed system into equation (A1-5), and using equation (A1-1), one obtains

$$(H^o - \underline{M}\,\underline{E})\Psi_k' = \frac{-h}{2\pi i}\,\frac{\partial \Psi_k'}{\partial t} + \underline{M}\,\underline{E}\,\Psi_k^o \qquad \text{(A1-7)}$$

where $\underline{M}\,\underline{E}\,\Psi_k'$ can be neglected as a second order term.

The general solution of equation (A1-7) can be written in the form

$$\Psi_k' = \Psi_k^+ \exp\left[\frac{-2\pi i}{h}(E_k + h\nu_o)t\right] + \Psi_k^- \exp\left[\frac{-2\pi i}{h}(E_k - h\nu_o)t\right] \qquad \text{(A1-8)}$$

which can be verified by direct substitution.

Substituting equations (A1-4, 8) into the wave equation for the perturbed system, and equating the coefficients of terms involving the same time dependence, results in the following set of equations

$$H^o\psi_k^+ - [E_k + h\nu_o] = \underline{A}\,\underline{M}\,\psi_k$$
$$H^o\psi_k^- - [E_k - h\nu_o] = \underline{A}\,\underline{M}\,\psi_k \qquad \text{(A1-9)}$$

Now the intermediate level $(h\nu_o + E)$ is not a stationary state of the molecule, but, by the usual perturbation theory of wave mechanics it can be described by a summation over all possible stationary energy levels; i.e., over all electronic, vibrational, and rotational levels.

Therefore, let

$$(\underline{A}\,\underline{M})\,\psi_k = \sum_r (\underline{A}\,\underline{M}_{kr})\,\psi_r \qquad \text{(A1-10)}$$

where $\underline{M}_{kr} = \int \psi_r^* \underline{M} \psi_k \, d\tau$ is the transition amplitude $(k \to r)$ in the unperturbed system, and r is some arbitrary intermediate energy level.

If one now considers the time dependent wave equation

$$H^o\psi_r = E_r\psi_r \qquad \text{(A1-11)}$$

then one can obtain for $\psi^{\pm}$ the following expressions

$$\psi_k^+ = \sum_r \frac{(\underline{A}\,\underline{M}_{kr})\,\psi_r}{E_r - E_k - h\nu_o} \quad ; \quad \psi_k^- = \sum_r \frac{(\underline{A}^*\underline{M}_{kr})\,\psi_r}{E_r - E_k + h\nu_o} \qquad \text{(A1-12)}$$

Therefore, the perturbed portion of the wave function can be written as

$$\Psi_k' = \frac{1}{h} \sum_r \psi_r \left\{ \frac{(\underline{A}\,\underline{M}_{kr})}{\nu_{rk} - \nu_o} \exp\left[\frac{-2\pi i}{h}(E_k + h\nu_o)t\right] + \frac{(\underline{A}^*\underline{M}_{kr})}{\nu_{rk} + \nu_o} \exp\left[\frac{-2\pi i}{h}(E_k - h\nu_o)t\right] \right\} \qquad \text{(A1-13)}$$

Now, the induced electric moment, M′ of the perturbed molecule can be written as

$$\underline{M}'_{kk}=\int \Psi^*_k \underline{M} \Psi_k d\tau \tag{A1-14}$$

Substituting for Ψ_k and neglecting the second order terms, results in

$$\underline{M}'_{kk}=\underline{M}^o_{kk} + \frac{1}{h}\sum_r \left\{\frac{(\underline{A}\,\underline{M}_{kr})\underline{M}_{rk}}{\nu_{rk}-\nu_o} + \frac{\underline{M}_{kr}(\underline{A}\,\underline{M}_{rk}}{\nu_{rk}+\nu_o}\right\}\exp\,[-2\pi i\nu_o t]$$
$$+\frac{1}{h}\sum_r \left\{\frac{(\underline{A}^*\underline{M}_{kr})\underline{M}_{rk}}{\nu_{kr}+\nu_o} + \frac{\underline{M}_{kr}(\underline{A}^*\underline{M}_{rk})}{\nu_{rk}-\nu_o}\right\}\exp\,[+2\pi i\nu_o t] \tag{A1-15}$$

The first term is time independent and represents the permanent dipole moment of the state k. The other terms are time dependent and of the same frequency as the incident radiation. These terms represent scattered radiation of the same frequency as the incident radiation and are termed Rayleigh scattering.

The total intensity of radiation arising from the electric moment can be written as

$$I=\frac{64\pi^4\nu_o^4}{3c^3}|\underline{E}_{kk}|^2 \tag{A1-16}$$

where $\underline{M}'_{kk}$ can be written in the form

$$\underline{M}'_{kk}=\underline{E}_{kk}\exp(-2\pi i\nu_o t) + \underline{E}^*_{kk}\exp(2\pi i\nu_o t) \tag{A1-17}$$

and therefore,

$$\underline{E}_{kk}=\frac{1}{h}\sum_r \left\{\frac{(\underline{A}\,\underline{M}_{kr})\underline{M}_{rk}}{\nu_{rk}-\nu_o} + \frac{\underline{M}_{kr}(\underline{A}\,\underline{M}_{rk})}{\nu_{rk}+\nu_o}\right\} \tag{A1-18}$$

Substituting equation (A1-18) into equation (A1-16), yields an equation for the total intensity of Rayleigh scattered light for one molecule.

Now, if the molecule makes a transition from level k to n, due to its interaction with the incident radiation, the resulting electric

moment is

$$\underline{M}'_{kn} = \int \Psi_n^* \underline{M} \Psi_k \, d\tau \tag{A1-19}$$

Repeating the above procedure, one obtains

$$\underline{M}' = \underline{M}_{kn} e^{-2\pi i \nu_{kn} t} + \frac{1}{h} \sum_r \left[\frac{(\underline{A}\,\underline{M}_{kr})\underline{M}_{rn}}{\nu_{rk} - \nu} + \frac{\underline{M}_{kr}(\underline{A}\,\underline{M}_{rn})}{\nu_{rn} + \nu} \right] e^{-2\pi i(\nu_{kn} + \nu)t}$$

$$+ \frac{1}{h} \sum_r \left[\frac{(\underline{A}^* \underline{M}_{kr})\underline{M}_{rn}}{\nu_{rk} + \nu} + \frac{\underline{M}_{kr}(\underline{A}^* \underline{M}_{rn})}{\nu_{rn} + \nu} \right] e^{-2\pi i(\nu_{kn} - \nu)t} \tag{A1-20}$$

The first terms refer to the spontaneous emission of a quantum and the second terms corresponds to scattered radiation of frequency $\nu_o + \nu_{kn}$, subject to the condition

$$\nu_o + \nu_{kn}, \; \nu_o - \nu_{kn} > 0 \quad \text{or} \quad E_n < E_k + h\nu_o \tag{A1-21}$$

where E_k and E_n are the energies of the initial and final states, respectively. This type of scattering is termed Raman scattering. If $E_n > E_k$, then the frequency of the scattered radiation is decreased, while the molecule gains the corresponding amount of internal energy. If $E_k > E_n$, then the frequency of the scattered radiation is increased and the molecule looses the corresponding amount of internal energy. In order for the latter process to occur, the state k must be an excited state. The resulting radiation due to the former phenomenon is termed Stokes radiation, while the latter is termed Anti-Stokes radiation.

The third terms refer to radiation for $\nu_{kn} - \nu_o > 0$ or $E_n < E_k - h\nu$. Therefore, if the incident frequency ν_o corresponds to visible or ultraviolet radiation, the initial state of the molecule should be an electronically excited state in order for the transition to occur. These

transitions have not yet been detected and therefore, this term will not be considered herein.

In similar manner, the electric moment can be written in the form

$$\underline{M}'_{kn} = \underline{E}_{kn} \exp[-2\pi i(\nu_{kn} + \nu)t] + \underline{E}^{*}_{kn} \exp[-2\pi i(\nu_{kn} - \nu)t] \qquad \text{(A1-22)}$$

where $$\underline{E}_{kn} = \frac{1}{h} \sum_r \left\{ \frac{(\underline{A}\ \underline{M}_{kr})\underline{M}_{rn}}{\nu_{rk} - \nu_o} + \frac{\underline{M}_{kr}(\underline{A}\ \underline{M}_{rn})}{\nu_{rn} + \nu_o} \right\} \qquad \text{(A1-23)}$$

and therefore, the total intensity of the Raman scattered radiation is of the form

$$I_{kn} = \frac{64\pi^4(\nu_o + \nu_{kn})^4}{3c^3} N|E_{kn}|^2 \qquad \text{(A1-24)}$$

where E_{kn} is given by equation (A1-23).

Therefore, the intensity of scattered radiation is determined by the emission or absorption frequencies and the transition amplitudes $\underline{M}_{kr}, \underline{M}_{rn}$. Since the intensity depends only on the amplitude and not its square (transition probability), different terms relating to the intermediate state will cancel or strengthen each other by interference.

The intermediate states, r, only contribute to the intensity if the transition (k→r) and the transitions (r→n) are allowed in ordinary absorption. If the intermediate level r does not exist, the Raman transition (k→n) is forbidden. Therefore, in terms of the quantum theory the difference between the Raman and absorption selection rules lies in the fact that the former corresponds to a double transition and the latter to a single direct transition between two states.

The intensity of scattered radiation from a group of molecules,

in a particular direction, can be expressed as

$$I_{kn}(\bar{q}) = \frac{8\pi^3(\nu_o + \nu_{kn})^4}{r^2c^3} N |E_{kn}(\bar{q})|^2 \qquad \text{(A1-25)}$$

where $\bar{q}$ is the unit vector in the direction of polarization along which the scattering is observed and r is the distance between the scattering system and an observer.

As can be seen, in order to evaluate the transition probability E_{kn} and, therefore, the intensity of scatter radiation, a sum over all the states must be performed. This is most difficult. Fortunately, under some restrictions, this can be accomplished using the concept of polarizability. This theory is described in the next appendix.

APPENDIX II

POLARIZABILITY THEORY

The evaluation of the transition probability (Eq. A1-23), over all states is very complicated. Fortunately, Placzek[8] devised a theory where, under certain restrictions, the evaluation over all the states is not necessary. An outline of this theory will be given in this Appendix. The presentation herein follows the material included in Refs. 8,10,13, and 25.

For a wide variety of physically interesting conditions, the total wave function of a molecular system can be separated with a good degree of accuracy, in the following manner:[27]

$$\psi = \psi_e \psi_v \psi_r \qquad \text{(A2-1)}$$

That is, the total wave function can be separated into components due to electronic, vibrational and rotational phenomena.

Therefore, the total energy can also be resolved into separate components E_e, E_v and E_r, where $E=E_v+E_e+E_r$ and $E_e > E_v > E_r$. Utilizing this approximation, the summation over the intermediate states, as given in Eq. (A1-23), can be more easily evaluated . Under the assumption that the frequency of the incident light quantum, ν_o, is much lower than the lowest electronic transition frequency of the molecule ν_e, (i.e., $\nu_o \ll \nu_e$), then the ground electronic state is the only electronic state which needs to be considered. If it is also assumed that the ground state is nondegenerate, and $\nu_o \gg \nu_v$, $\nu_e - \nu_o \gg \nu_v$, where ν_v is the frequency of the molecular vibration, the sum over the ground state wave functions can be replaced by the polarizability of the molecule with fixed nuclei, and by the effect of the nuclear motions on the polarizability.

When a photon interacts with a molecule, the oscillating electric field $\underline{E}$ of the incident radiation induces a dipole moment $\underline{P}$ in the molecule. That is, the relative positions of the charges in the molecule are displaced from their equilibrium positions producing a diple moment of magnitude

$$|\underline{P}| = \hat{\alpha}\,|\underline{E}| \tag{A2-2}$$

where $\hat{\alpha}$ is the polarizability tensor which is assumed to be independent of $\underline{E}$. Comparing this representation to that in the previous appendix, we see that, for a typical component of $\underline{E}_{kn}$, the following relationship holds

$$(E_x)_{kn} = \sum_y (\alpha_{xy})_{kn} A_y \tag{A2-3}$$

where

$$(\alpha_{xy})_{kn} = \frac{1}{h} \sum_r \left\{ \frac{(M_y)_{kr}(M_x)_{rn}}{\nu_{rk} - \nu} + \frac{(M_x)_{kr}(M_y)_{rn}}{\nu_{rn} + \nu} \right\} \tag{A2-4}$$

Thus, under the previously outlined assumptions, the polarizability tensor has in effect replaced the sum over all the states. This representation is useful since $\hat{\alpha}$ can be determined experimentally.

The polarizability tensor is a symmetric tensor (i.e., $\alpha_{ij} = \alpha_{ji}$) and its components ($\alpha_{xx}$, α_{xy}, etc) are referred to a coordinate system x, y, z fixed in the molecule. The tensor can be represented by an ellipsoid with principal axes fixed in the molecule, along which both $\underline{P}$ and $\underline{E}$ have the same direction. In general, the polarizability ellipsoid has the same symmetry as the charge distribution, which almost always follows the symmetry of the nuclear frame. Thus, any axis of symmetry of a molecule is a principal axis of the ellipsoid and any plane of symmetry contains two axes of the ellipsoid. When all three axes of the ellipsoid are equal, as in spherical top molecules, the

polarizability is isotropic. When at least two of the axes are different, as in linear, symmetric top, and asymmetric top molecules, the polarizability is anisotropic.

The polarizability will, of course, vary with the vibrational and rotational motions of the molecules. For vibrational motion of infinitesimal amplitudes, the polarizability can be represented by an expansion of terms of the 3N-6 normal coordinates q_i. A typical component is of the form

$$\alpha_{xy} = \alpha_{xy}^{o} + \sum_{i=1}^{3N-6} \left\{ \frac{\partial \alpha_{xy}}{\partial q_i} \right\}_e q_i + \text{H.O.T.} \qquad \text{(A2-5)}$$

The first term represents the polarizability of the equilibrium position and the second term represents the linear change in polarizability with the normal coordinates at the equilibrium position. These two terms give the polarizability in accordance with the harmonic oscillator approximation. The higher terms are those due to electrical anharmonicity.

When the rotational motions of the molecule are considered, the polarizability must be expressed in a space-fixed coordinate system (X, Y, Z). The components in this system are given in terms of the polarizability components along the x, y, z axes fixed in the molecule. A typical component of the polarizability tensor in the X, Y, Z system is of the form

$$\alpha_{XY} = \sum_{x,y} \alpha_{xy} \cos(x, X) \cos(y, Y) \qquad \text{(A2-6)}$$

where α_{xy} is a function of the normal coordinates only, and is independent of the rotational state and the orientation of the molecule. The direction cosines are functions of the Eulerian angles.

Now, in order to determine the selection rules and intensities of Raman transitions according to wave mechanics, the transition

probabilities must be calculated. Therefore, one must consider the matrix elements of the induced dipole moment

$$[\underline{P}]_{kn} = \int \Psi_k \underline{P} \Psi_n^* d\tau \qquad \text{(A2-7)}$$

where Ψ_k and Ψ_n are the time-dependent eigenfunctions of two states, k and n, of a molecule. As can be readily seen in Appendix I, the components of the matrix $[\underline{P}]_{kn}$ with indices n=k correspond to Rayleigh scattering, since they vary with the frequency ν_o, and the components with indices n≠k correspond to Raman scattering with frequency $\nu_o + (E_k - E_n)/h$. (Here, of course, $\underline{P}$ has been used in place of $\underline{M}$ in order to denote the use of the polarizability approximation).

The time independent part of the induced dipole moment is

$$[P^o]_{kn} = \int \psi_k P^o \psi_n^o d\tau \qquad \text{(A2-8)}$$

where the components of P^o are of the form

$$[P_i^o]_{kn} = \sum_j [\alpha_{ij}]_{kn} E_j^o \qquad \text{(A2-9)}$$

where i, j=x, y, z and

$$[\alpha_{ij}]_{kn} = \int \alpha_{ij} \psi_n^* \psi_k d\tau \qquad \text{(A2-10)}$$

Since the square of $[P^o]_{kn}$ is proportional to the transition probability from state k ↔ n, if any one of these matrix elements is different from zero, a Raman transition k↔n is allowed.

Now, $\psi_{k,n}$ are the time independent wave function amplitudes which obey Schrodinger's wave equation. In the context of the polarizability theory, they can be rewritten as

$$\psi_{k,n} = (\psi_v)_{k,n} (\psi_r)_{k,n} \qquad \text{(A2-11)}$$

where $(\psi_v)_{k,n}$ and $(\psi_r)_{k,n}$ are the vibrational and rotational wave function amplitudes, respectively, in the states k or n.

Substituting the appropriate relations (Eqs. (A2-10,11)) into Equation A2-9, one obtains for $[P_i^o]_{kn}$ the following expression

$$[P_i^o]_{kn} = \sum_j \left\{ E_j^o \int (\psi_v)_k (\psi_r)_k \alpha_{ij} (\psi_v^*)_n (\psi_r^*)_n d\tau \right\} \qquad \text{(A2-12)}$$

Therefore, given ψ_v, ψ_r one can solve for the transition probabilities and the intensity of in terms of α_{ij}. In order to determine ψ_v and ψ_r, a molecular model must be assumed and the corresponding wave equation solved. In the following discussion the harmonic oscillator and rigid dumbbell models will be assumed. For details on solving for ψ_v and ψ_r utilizing these molecular models, see Ref. 25.

Consider first, the vibrational motions only. Substituting Eq. (A2-5) into eq. (A2-10), and neglecting higher order terms, results in

$$[\alpha_{xx}]_{kn} = (\alpha_{xx})_e \int (\psi_v)_k (\psi_v)_n d\tau + \frac{1}{i} \left(\frac{\partial \alpha_{xx}}{\partial q_i} \right)_e \int (\psi_v^*)_k q_i (\psi_v) d\tau \qquad \text{(A2-13)}$$

in which ψ_k and ψ_n are functions of all the q_i. Due to the orthogonality properties of the wave functions, the first term is zero, unless the vibrational states are the same (i.e., unless k=n) and therefore, does not contribute to the vibrational intensity. The second term is equal to zero only if the quantum numbers correspoinding to the states k and n do not differ by ± 1 or if $(\partial \alpha_{xx}/\partial q_i)_e$ is equal to zero.

Therefore, for the harmonic oscillator approximation, only fundamental frequencies can occur and only those frequencies which produce a change in polarizability. If higher order terms were kept, then overtone and combination frequencies could occur, but the intensities corresponding to these frequencies are very small in amplitude, as compare to the intensity corresponding to the fundamental frequency.

Therefore, for vibrational Raman scattering, one has

$$[\alpha_{xx}]_{kn}=\left[\frac{\partial\alpha_{xx}}{\partial q_i}\right]_e\int(\psi_v^*)_k q_i(\psi_v)_n\,d\tau \qquad (A2\text{-}14)$$

Substituting the eigenfunctions of harmonic oscillator, results in

$$[\alpha_{xx}]_{kn}=\alpha'_{xx}\left[\frac{h}{8\pi^2\mu\omega_e}\right] \qquad (A2\text{-}15)$$

where $\alpha'_{xx}=(\partial\alpha_{xx}/\partial q_i)_e$. Thus, the polarizability tensor, in the x direction, is of the form

$$[P_x]_{kn}=\left[\frac{h}{8\pi^2\mu\omega_e}\right]^{\frac{1}{2}}[E_x\alpha'_{xx}+E_y\alpha'_{xy}+E_z\alpha'_{xz}] \qquad (A2\text{-}16)$$

If we now consider the rotational motions of the molecule we must transform to a coordinate system fixed in space. This relation is given by

$$\alpha_{XY}=\sum_{xy}\alpha_{xy}\cos(x,X)\cos(y,Y) \qquad (A2\text{-}6)$$

Therefore, one can write the matrix element of the polarizability tensor for a vibrating rotating molecular system as (See Eqs. (A2-10,11))

$$[\alpha_{XY}]_{nm}=\int(\psi_v)_n\alpha_{xy}(\psi_v^*)d\tau_v\int(\psi_r)_n\cos(x,X)\cos(y,Y)(\psi_r^*)_k d\tau_r \qquad (A2\text{-}17)$$

where α_{xy} is given by Eq. (A2-5). Since at ordinary temperatures the rotational energies are normally excited, the transformation to the fixed coordinate system X, Y, Z can simply be made by averaging in the classical sense, over all orientations of the molecule. This averaging process must be made of all the squares and crossproducts of the tensor components over all orientations of the tensor ellipsoid. This type of averaging is not necessary, since the substitution of the rotational wave function as given in Ref. 25 into equation (A2-17) will give the same result. It is used herein, since it is convenient.

It is convenient to introduce two invariants of the polarizability

tensor. In the general case of anisotropic polarizability the tensor α has two invariants defined as the spherical (or isotropic) part of the polariability, α, and anisotropic part γ^2, where

$$\alpha = 1/3(\alpha_{XX} + \alpha_{YY} + \alpha_{ZZ}) \tag{A2-18}$$

$$\gamma^2 = 1/2\,[(\alpha_{XX}-\alpha_{YY})^2 + (\alpha_{YY}-\alpha_{ZZ})^2 + (\alpha_{ZZ}-\alpha_{XX})^2 + 6(\alpha_{XY}^2 + \alpha_{YZ}^2 + \alpha_{ZX}^2)] \tag{A2-19}$$

In accordance with this representation, one can define invariants of the polarizability derivate tensor, α', where the derivatives replace their respective components in Eq.s (A2-18,19) (i.e., $\alpha_{ij} \rightarrow \partial\alpha_{ij}/\partial q_i$). The invariants α and γ^2 appear in formulations related to Rayleigh scattering, while α' and γ'^2 appear in those relations describing Raman scattering.

The averaging (see Ref. 13) described in Eq. (A2-6) results in the following set of relationships between α'_{ij} and the invariants α, γ^2 of the polarizability derivative tensor:

$$\overline{(\alpha'_{ii})^2} = \frac{1}{45}(45\alpha'^2 + 4\gamma'^2) \tag{A2-20}$$

$$\overline{(\alpha'_{ij})^2} = \frac{3\gamma'^2}{45} \tag{A2-21}$$

For Rayleigh scattering one would only have to omit the derivative notation in order to obtain the correct relations.

Using these relationships, the scattered intensity, as a function of viewing angle with respect to the incident radiation, can be derived for various modes of polarized incident radiation. Therefore, the intensity of the scattered radiation can be written in the form

$$I = \frac{C\omega(\nu_o + \nu_{kn})^4}{c^3} N|P_{kn}|^2 \tag{A2-22}$$

where N is the number of molecular scatterers in the state k and $|P_{kn}|^2$ is a function of θ, α', and γ' as defined by Eqs. (A2-16, 20, 21).

It is seen from Eq. (A2-20, 21) that the intensity of Raman scattering is made up of two parts; one due to isotropic scattering (i.e., proportional to α'^2) and one due to anisotropic scattering (i.e., proportional to γ'^2). The specific relationship for $|P_{nm}|^2$ will be derived for a number of interesting cases in the next appendix.

As stated previously, the intensity relationship for Rayleigh scattering can be obtained for the above presentation by recognizing that if k=n, all results derived above, correspond to Rayleigh scattering wherein α' and γ'^2 must be replaced by α and γ^2.

The intensity as derived above (Eq. (A 2-22)), includes the contributions from all of the rotational transitions and , therefore, represents the intensity of the entire Raman vibrational-rotational band. The contribution of the rotational transitions have been derived utilizing a sum, in the classical sense, over all rotational states. The same result can be obtained utilizing the wave functions amplitudes for the rotational levels and evaluating the appropriate transition probabilities (see Ref. 8,9). This has not been included herein, since these results are quite involved due to the many variations in quantum conditions. The intensity of the scattered radiation due to a rotational transition can be derived utilizing this approach and is of the following form

$$I_{rot}=C_3(\nu_o + \nu_{JJ'})^4 \, g_J N \, b^{JK}_{J'K'} \qquad (A2\text{-}23)$$

where C_3 is a constant and the specific values for g_J and $b^{JK}_{J'K'}$ are given in Ref. 8-10.

In some applications, it may be more advantageous to observe the Q-branch of the vibrational-rotational band(see Appendix IV for a description of the Q-branch). In this case, the intensity of the Q-branch

is of the form

$$I_{rot} = \frac{64\pi^4}{3c} (\nu_o + \nu_{kn})^4 \, N |P_{kn}|^2 \qquad \text{(A2-24)}$$

where $|P_{kn}|^2$ is now a function of χ as well; where χ is the fraction of the anisotropic intensity in the Q-branch and is given by

$$\chi = \frac{1}{Z_J} \sum_J g_J (2J+1) \exp\left[\frac{-J(J+1)hBc}{kT}\right] \frac{J(J+1)}{(2J-1)(2J+3)} \qquad \text{(A2-25)}$$

where Z_J is the rotational partition function. For low values of hBc/kT, χ is equal to .25 for O_2, N_2, D_2, and is equal to 0.32 for H_2 (at room temperature).

The relationship for $|P_{kn}|^2$, as derived in Appendix IV, are for the entire band and include the factor χ in the appropriate terms in order to allow the determination of the intensity of the Q-branch. Since most investigations involving the determination of the polarizability invariants observe the Q-branch only, an understanding of χ is necessary in order to obtain the proper interpretation of their results with respect to the measurement made herein.

APPENDIX III

TRANSITION AMPLITUDE AND DEPOLARIZATION RATIO

Consider an experimental configuration, wherein the incident radiation is directed along the Z axis, as defined in the coordinate system depicted below:

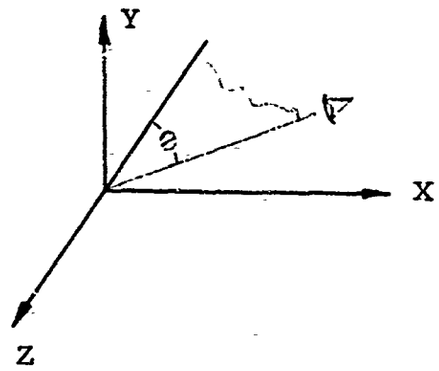

and the observation of the scattered radiation is made at some arbitrary angle, θ, to the Z axis in the XZ plane. Also, consider the following modes of polarization of the incident radiation.

$$\text{I)} \quad E_X = |E|; \quad E_Y = E_Z = 0$$

$$\text{II)} \quad E_Y = |E|; \quad E_X = E_Z = 0$$

$$\text{III)} \quad E_X = E_Y = |E|; \quad E_Z = 0$$

The general relationship for a component of the transition amplitude directed along a coordinate axes, for a randomly oriented molecular scattering system, is of the form (See Appendix II)

$$[P_i]_{kn}^2 = \frac{h}{8\pi^2 \mu \omega_e} \sum_j \overline{(\alpha'_{ij})^2} E_j^2 \qquad \text{(A3-1)}$$

where i, j=X, Y, Z and

$$\overline{(\alpha'_{ii})^2} = \frac{1}{45}(45\alpha'^2 + 4\gamma'^2\chi); \quad \overline{(\alpha'_{ij})^2} = \frac{3\gamma'^2\chi}{45} \qquad \text{(A3-2)}$$

Here $\chi = 1$ for the entire vibrational-rotational band and is given by Eq. A2-25 for the Q-branch.

For an arbitrary viewing angle, θ, with respect to the incident radiation, the transition amplitude can be written in terms of these components, in the following manner:

$$[P_\theta]^2=[P_X]^2\cos^2\theta + [P_Y]^2 + [P_Z]^2\sin^2\theta \qquad (A3-3)$$

Utilizing these relationships, the transition amplitude, for the different modes of polarization of the incident radiation, can be written as

Case I Horizontally polarized radiation

$$[P_\theta]^2=K[45\alpha'^2 + 7\gamma'^2\chi)\cos^2\theta + 6\gamma'^2\chi\sin^2\theta] \qquad (A3-4)$$

Case II Vertically polarized radiation

$$[P_\theta]^2= K[45\alpha'^2 + 7\gamma'^2\chi] \qquad (A3-5)$$

Case III Unpolarized radiation

$$[P_\theta]^2=K[(45\alpha'^2+7\gamma'^2\chi)(1+\cos^2\theta)+6\gamma'^2\chi\sin^2\theta] \qquad (A3-6)$$

where $K= \frac{h}{8\pi\mu\omega_e^4 45} = \frac{8\pi B_e r_e^2 I_o}{45\omega_e}$

In a similar manner, one can derive thevariation of the depolarization ratio, ρ, with observation angle θ, for the different modes of polarization considered . The depolarization ratio, ρ, is defined as:

$$\rho = I_\perp / I_{\parallel} \qquad (A3-7)$$

where $I_\perp$ and $I_{\parallel}$ are, respectively, the intensities of the components of scattered light with electric vectors vibrating in the directions perpendicular and parallel to that of the incident light.

I Horizontally Polarized Radiation

$$\rho= \frac{(45\alpha'^2 + 4\gamma'^2\chi)\cos^2\theta + 3\gamma'^2\sin^2\theta}{3\gamma'^2\chi} \qquad (A3-8)$$

II Vertically Polarized Radiation

$$\rho= \frac{3\gamma'^2\chi}{45\alpha'^2 + 4\gamma'^2\chi} \qquad (A3-9)$$

III Unpolarized Radiation

$$\rho = \frac{(45\alpha'^2 + 7\gamma'^2\chi)\cos^2\theta + 6\gamma'^2\chi \sin^2\theta}{45\alpha'^2 + 7\gamma'^2\chi} \qquad \text{(A 3-10)}$$

APPENDIX IV

DETERMINATION OF THE RAMAN FREQUENCY SHIFTS

Since the Raman shift occurs due to an energy exchange between the incident photon and the irradiated molecule, a determination of the various stationary energy states of the molecule can be used to determine the corresponding Raman shift. As stated in the text, most observed Raman shifts result from vibrational-rotational transitions and therefore, only these transitions will be considered here.

In order to predict the energy levels accurately and to adequately determine the fine structure, the molecular models utilized to determine the Raman frequency shifts should consider the interaction of the rotational and vibrational motions. That is, during vibration the internuclear distance changes and therefore the moment of inertia changes, affecting the rotation. Also, during rotation the centrifugal forces effect the vibrational motion. Therefore, in order to calculate the energy levels of a given molecule, the vibrating rotator model for a diatomic molecule will be used. This refinement is not absolutely necessary in most investigations which observe the entire vibrational-rotational band but, is included herein in order to be more general. It is most useful in determining the wavelength and spacing of the individual lines in the vibrational-rotational band as well as the total band width. This becomes necessary when one is interested in resolving individual lines comprising the band.

The term values of a vibrating rotator are[23]

$$T=\frac{E}{hc}=\omega_e\left(v+\tfrac{1}{2}\right)-\omega_e x_e\left(v+\tfrac{1}{2}\right)^2+\omega_e y_e\left(v+\tfrac{1}{2}\right)^3+\ldots.$$
$$+B_v J(J+1)-D_v J^2(J+1)^2+\ldots \qquad \text{(A4-1)}$$

where B_v is the mean rotational constant in the vibrational state considered and is related to B_e, the equilibrium rotational constant, in the following manner:

$$B_v = B_e - \alpha_e(v+\tfrac{1}{2}) + \ldots \qquad \text{(A4-2)}$$

where

$$B_e = h/(8\pi^2 c\mu r_e^2) \text{ and } B_e >> \alpha_e$$

In a similar manner, D_v represents the influence of the centrifugal force in the vibrational state v and is given by

$$D_v = D_e + \beta_e(v+\tfrac{1}{2}) + \ldots \qquad \text{(A4-3)}$$

where

$$D_e = \frac{4B_e^3}{\omega_e^2} \text{ and } D_e >> \beta_e$$

The change is wave number, due to a vibrational and rotational energy change, can be written in terms of the difference in the term values of the vibrating rotator in the following manner:

$$T' - T = \frac{1}{hc}(E' - E) = \bar{\nu} \qquad \text{(A4-4)}$$

where the prime represents the upper energy state considered. The various molecular constants described above are listed in Table V for some molecules of interest.

The vibrational selection rule for Raman scattering is (see Appendix II and Ref. 23),

$$\Delta v = \pm 1 \qquad \text{(A4-5a)}$$

while the rotational selection rule is

$$\Delta J = 0, \pm 2 \qquad \text{(A4-5b)}$$

Depending upon the rotational quantum jump considered, various different bands can be obtained for a given vibrational change. These bands are called the S, O, and Q branches, which correspond to $\Delta J = +2$,

-2, 0, respectively.

For the v= 0→v=1, vibrational transition (the one considered herein), the difference between $B_{v=0}$ and $B_{v=1}$ is very small; therefore, all the lines of the Q-branch are very close to each other and except with a high resolving spectrograph, are usually not resolved. This gives rise to an intense line near the vibrational line. The S and O branches are much weaker since their lines are not superimposed.

In most investigations[13-17] of the Raman effect, the Q-branch is observed. A schematic representation of these branches as they would be observed on an exposed spectroscopic plate is shown below.

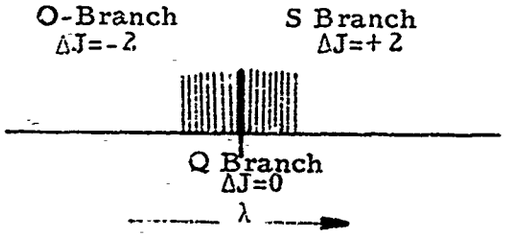

RAMAN VIBRATIONAL-ROTATIONAL BAND

The frequency of the Raman components can also be evaluated utilizing experimentally determined values of the Raman shift. These reported values usually are for the Q-branch, and therefore, in order to obtain the width and spacing of the vibrational-rotational bands, the type of calculation described above is useful. The Raman frequencies for CO_2 and CH_4 were determined in this manner from the data in Ref. 15. For applications of the Raman effect as demonstrated herein, this manner of determining Raman wavelengths is a quick and accurate enough technique to use.

The Raman frequency shifts, as calculated and utilized herein, for some molecules of interest are listed in Table (II). These are for

the Q-branch, where the rotational transition $J=0 \rightarrow J=0$ is considered. The Raman wavelengths can now be calculated using the equations for the index of refraction of air (n) as given in Appendix V.

APPENDIX V

INDEX OF REFRACTION OF AIR

In order to compute the wavelength of the various Raman lines as observed in air, a knowledge of the variation of the index of refraction of air, as a function of wavelength, temperature, and pressure must be known. The variation of the index of refraction with wavelength is given, for standard air (dry, 0.03 percent CO_2), by[24]

$$(n_{15,760}-1)10^8 = 6432.8 + \frac{2949810}{(146-\sigma^2)} + \frac{25540}{(41-\sigma^2)} \qquad \text{(A5-1)}$$

where $\sigma = \nu(10)^{-4}$ = wave number in vacuum in μ^{-2}

The variation of n with temperature and pressure is given by[24]

$$n_{TP}-1 = \frac{(n_{15,760}-1)P\ (1+P\beta_T)(1+15\eta)}{760\ (1+760\beta_{15})(1+\eta T)} \qquad \text{(A5-2)}$$

where: n_{TP} is the index of refraction of air at the desired temperature and pressure

$n_{15,760}$ is given by Equation A5-1

P is the pressure (Torr)

$\beta_T = (1.049-0.0157T)10^{-6}$

T is the temperature in ^{o}C

$\beta_{15} = 0.8135(10)^{-6}$

$\eta = 0.00366_1$

TABLE I

RAMAN SHIFTS AND POLARIZABILITY INVARIANTS

SPECIE	RAMAN SHIFT (cm^{-1})	ρ +	$\chi(\gamma'/\alpha')^2$	$\alpha'(10)^{16}\ cm^2$
O_2	155.6.2	$0.115^{(15)}$ Q $0.33^{(15)}$ $0.26^{(16)}$	1.0 4.02	$1.46^{(15)}$ $1.4^{(16)}$
N_2	2330.7	$0.055^{(15)}$ Q $0.180^{(15)}$ $0.190^{(16)}$	0.44 1.71	$1.75^{(15)}$ $1.60^{(16)}$
$CO_2(\upsilon_1)$	$1265^{(15)}$ $1285^{(15)}$ $1388^{(15)}$ $1409^{(15)}$	$0.250^{(15)}$ Q $0.084^{(15)}$ Q $0.054^{(15)}$ Q $0.150^{(15)}$ Q $0.14^{(15)}$ / $0.2^{(16)}$	2.65 0.699 0.432 1.364 $1.255^{(15)}$	$4.2^{(16)}$
$CH_4(\upsilon_1)$	$2914^{(15)}$	$0.0^{(15)}$ $0.0^{(16)}$	0.0	$4.16^{(15)}$ $4.10^{(16)}$
H_2	4159.24	$0.0732 \pm 0.00952^{(17)}$ $0.140^{(16)}$ $0.07^{(15)}$		$1.30 \pm 0.104^{(17)}$ $1.20^{(16)}$ $1.23^{(15)}$
CO	2143.3	$0.1040^{(15)}$ Q $0.310^{(15)}$		$1.50^{(15)}$

+ FOR UNPOLARIZED INCIDENT RADIATION AND TRANSVERSE (90°) OBSERVATION

NUMBER IN ( ) INDICATES REF. FROM WHICH DATA WAS OBTAINED

Q INDICATES Q BRANCH

TABLE II

MOLECULAR DATA AND RELATIVE RAMAN STOKES INTENSITIES

SPECIE	RAMAN SHIFT (cm^{-1})	α' ($10^{16} cm^2$)	$\chi(\gamma'/\alpha')^2$	$I_s/I_{s_{O_2}}$ (THEORY)	$I_s/I_{s_{O_2}}$ (SPECTRO.)	$I_s/I_{s_{O_2}}$ (FILTERS)
O_2	1556.2	1.46	4.02	1.0	1.0	1.0
N_2	2330.7	1.75	1.71	0.668	0.643	0.74
CO_2	1265 1285 1388 1409	4.20	1.26	1.97	2.32	1.87

TABLE III

VIBRATIONAL TEMPERATURE MEASUREMENTS

SPECIE	PRESSURE (TORR)	I_S / I_A EXPER.	T°K ACTUAL	T°K MEASURED	%ERROR
O_2	760	248	300.65	350	17
O_2	760	528	300.65	313.5	4.3
O_2	760	218	300.65	358	19
O_2*	760	567	300.35	310.4	3.4
O_2*	760	983	300.35	288.5	-4

* USING NARROW BANDPASS FILTERS (D=2.5mm)

TABLE IV

RAMAN TO RAYLEIGH INTENSITY RATIO

SPECIE	RAMAN SHIFT (cm^{-1})	$\frac{I_S}{I_R}\frac{\upsilon_0^4}{(\upsilon_0-\upsilon)^4}(10)^3$	
		(THEORY)	(THIS WORK)
O_2	1556.2	1.90	1.93
N_2	2330.7	1.32	1.19
CO_2	1265 1285 1388 1409	1.13	0.57
CH_4	2914	3.29	2.92

TABLE V

MOLECULAR CONSTANTS

MOLECULE	ω_e cm^{-1}	$\omega_e x_e$ cm^{-1}	$\omega_e y_e$ cm^{-1}	B_e cm^{-1}	α_e cm^{-1}	β_e cm^{-1}	r_e 10^{-8}cm
N_2	2359.61	14.456	0.00751	2.010	0.0187	$-1.0(10)^{-9}$	1.094
O_2	1580.361	12.073	0.0546	1.44566	0.01579	$-8.8(10)^{-8}$	1.2074
H_2	4395.24	117.99	0.293	60.80	2.993	$-1.34(10)^{-3}$	0.7417
NO	1904.03	13.97	-0.0012	1.7046	0.0178		1.1508
CO	2170.21	13.461	0.0308	1.9313	0.017485	$4.0(10)^{-8}$	1.1282
N_2^+	2207.19	16.136	-0.040	1.9322	0.0202	$2.9(10)^{-7}$	1.1162
O_2^+	1876.4	16.53		1.6722	0.01984		1.1227
H_2^+	2297.0	62.0		29.8	1.40		1.060

DATA OBTAINED FROM TABULATIONS LISTED IN REF. 23

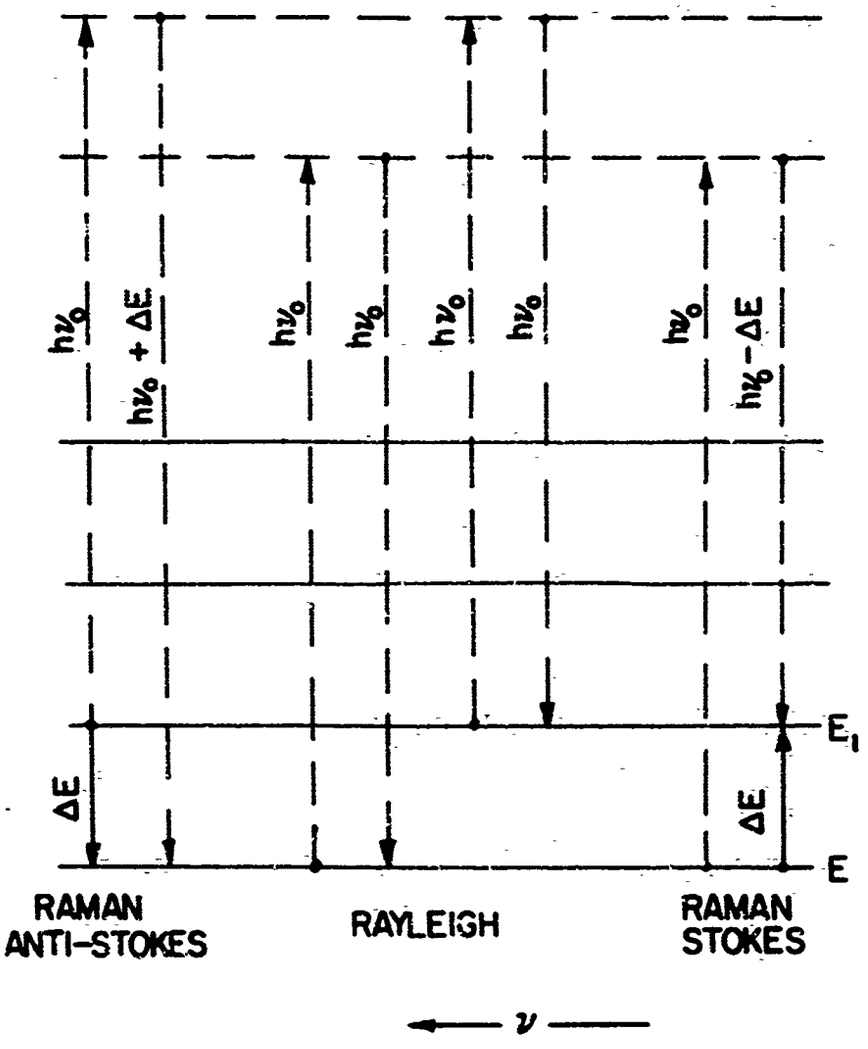

FIG.1 ENERGY LEVEL DIAGRAM SHOWING THE TRANSITIONS OCCURING IN A MOLECULE FOR RAYLEIGH AND RAMAN SCATTERING. THE SOLID LINES REPRESENT THE ACTUAL ENERGY LEVEL TRANSITIONS WHILE THE DASHED LINES REPRESENT VIRTUAL TRANSITIONS.

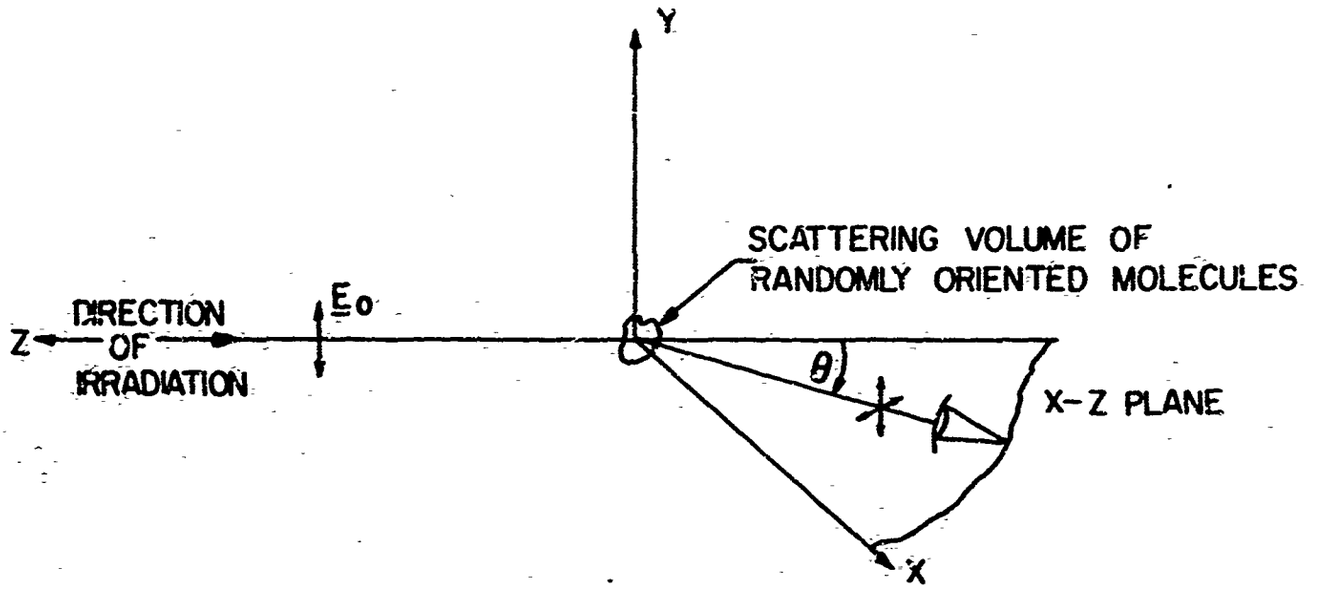

FIG. 2 COORDINATE SYSTEM SHOWING THE DIRECTION OF LASER IRRADIATION AND THE ORIENTATION OF THE VIEWING SYSTEM (THE LASER RADIATION IS VERTICALLY POLARIZED)

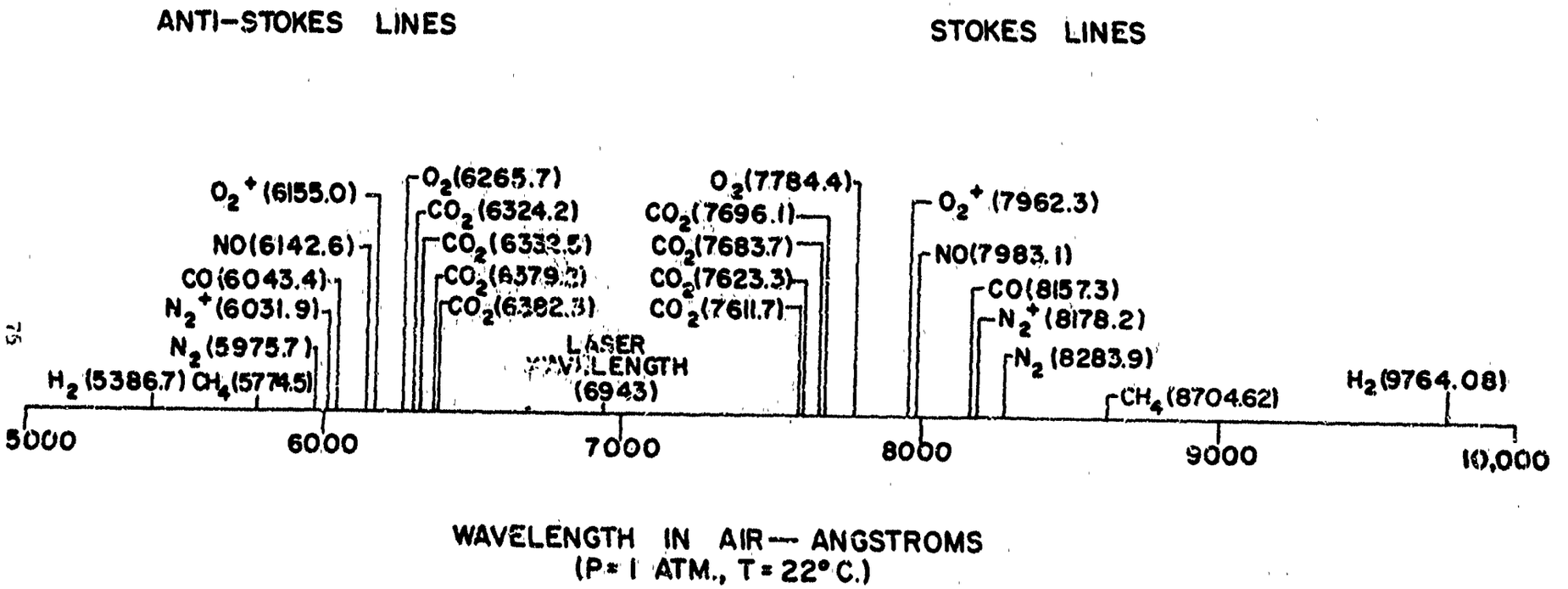

FIG. 3 WAVELENGTHS OF RAMAN SCATTERED RADIATION FOR VARIOUS MOLECULES EXCITED BY A RUBY LASER (6943 Å) AS MEASURED IN AIR

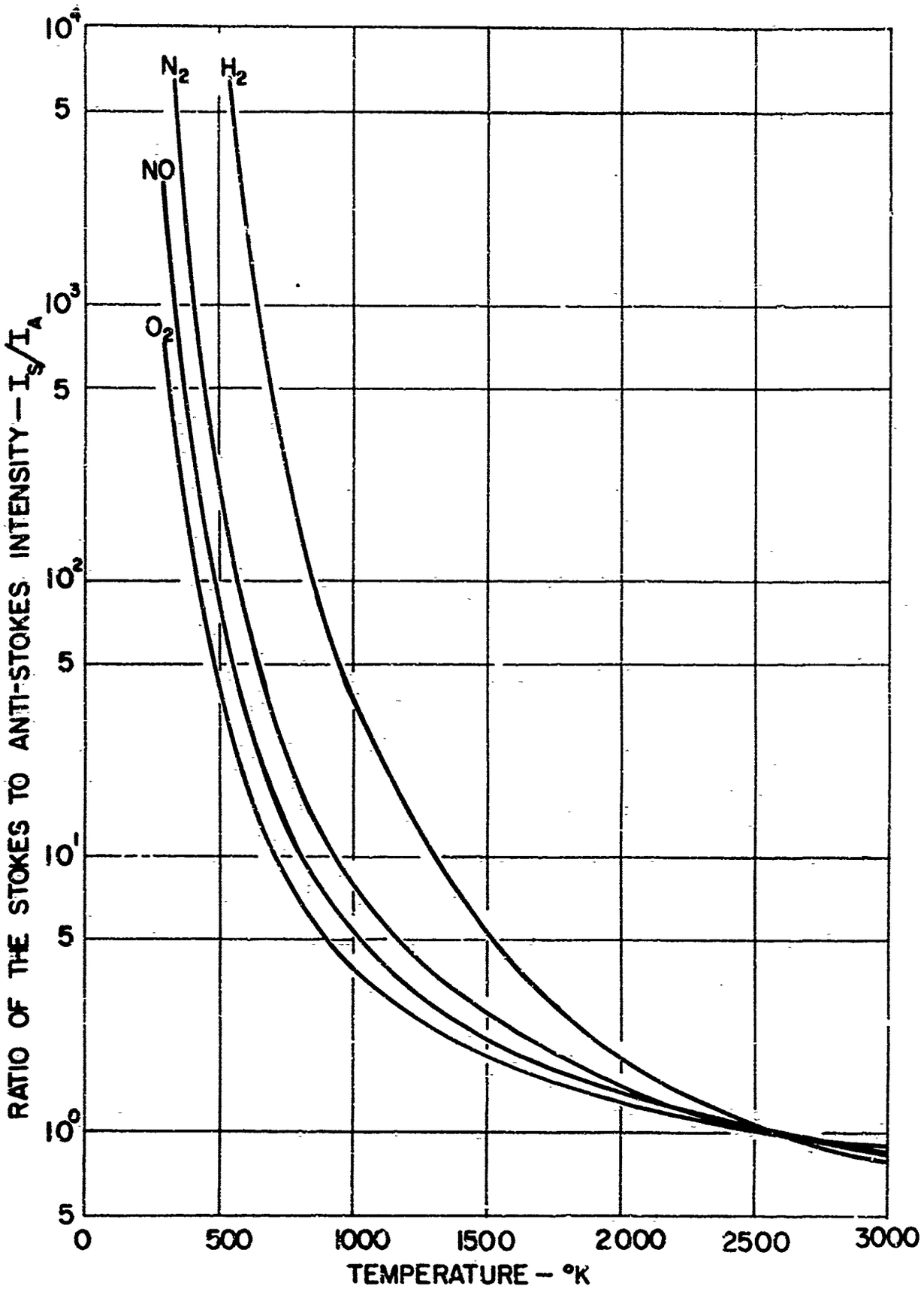

FIG.4 RATIO OF THE STOKES TO ANTI-STOKES INTENSITY AS A FUNCTION OF GAS TEMPERATURE FOR SOME MOLECULES OF INTEREST

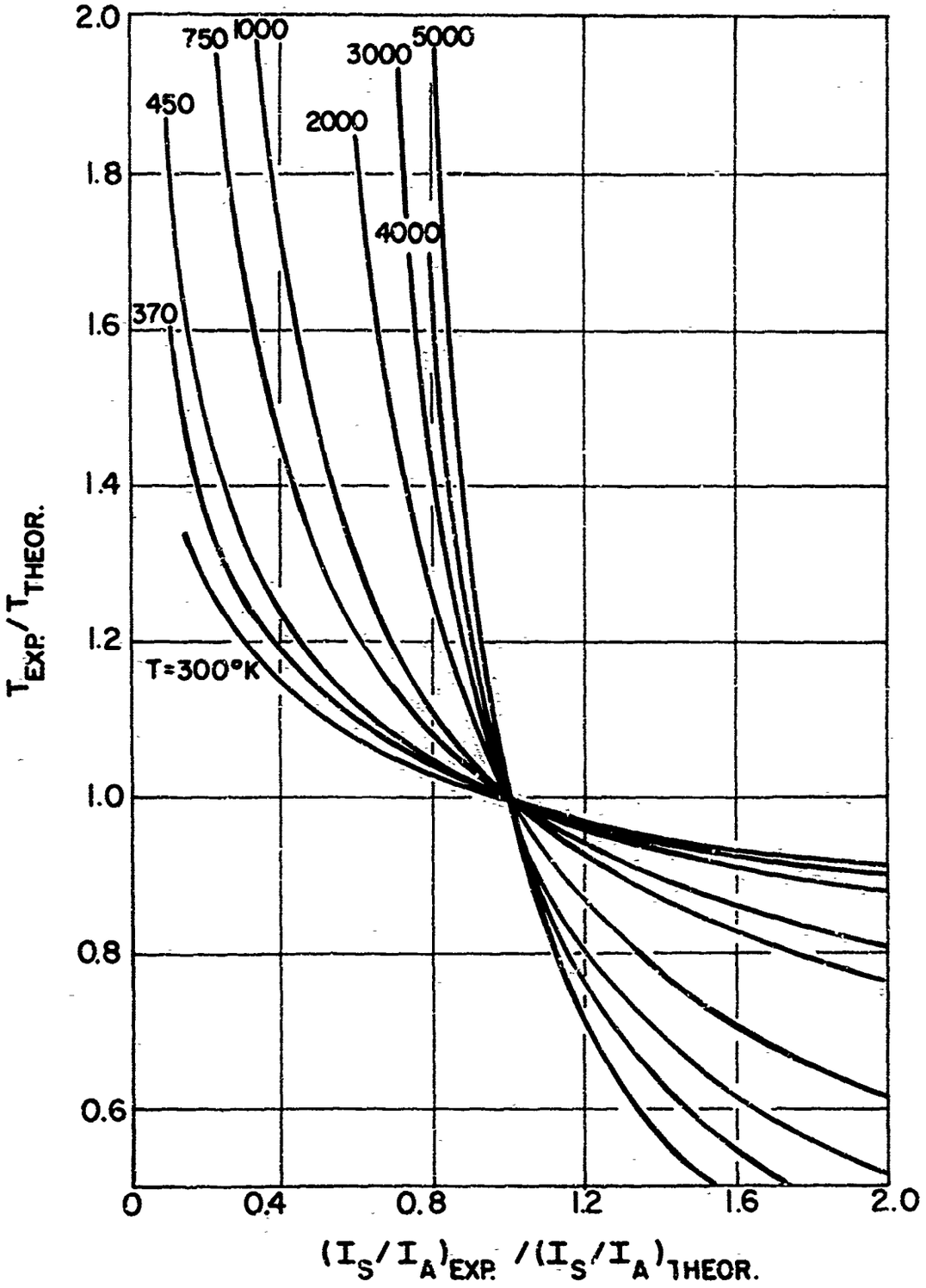

FIG. 5 THE RELATIVE CHANGE IN THE VIBRATIONAL TEMPERATURE OF O_2 AS A FUNCTION OF THE CHANGE IN THE MEASUREMENT OF THE RATIO OF THE STOKES TO ANTI-STOKES INTENSITIES

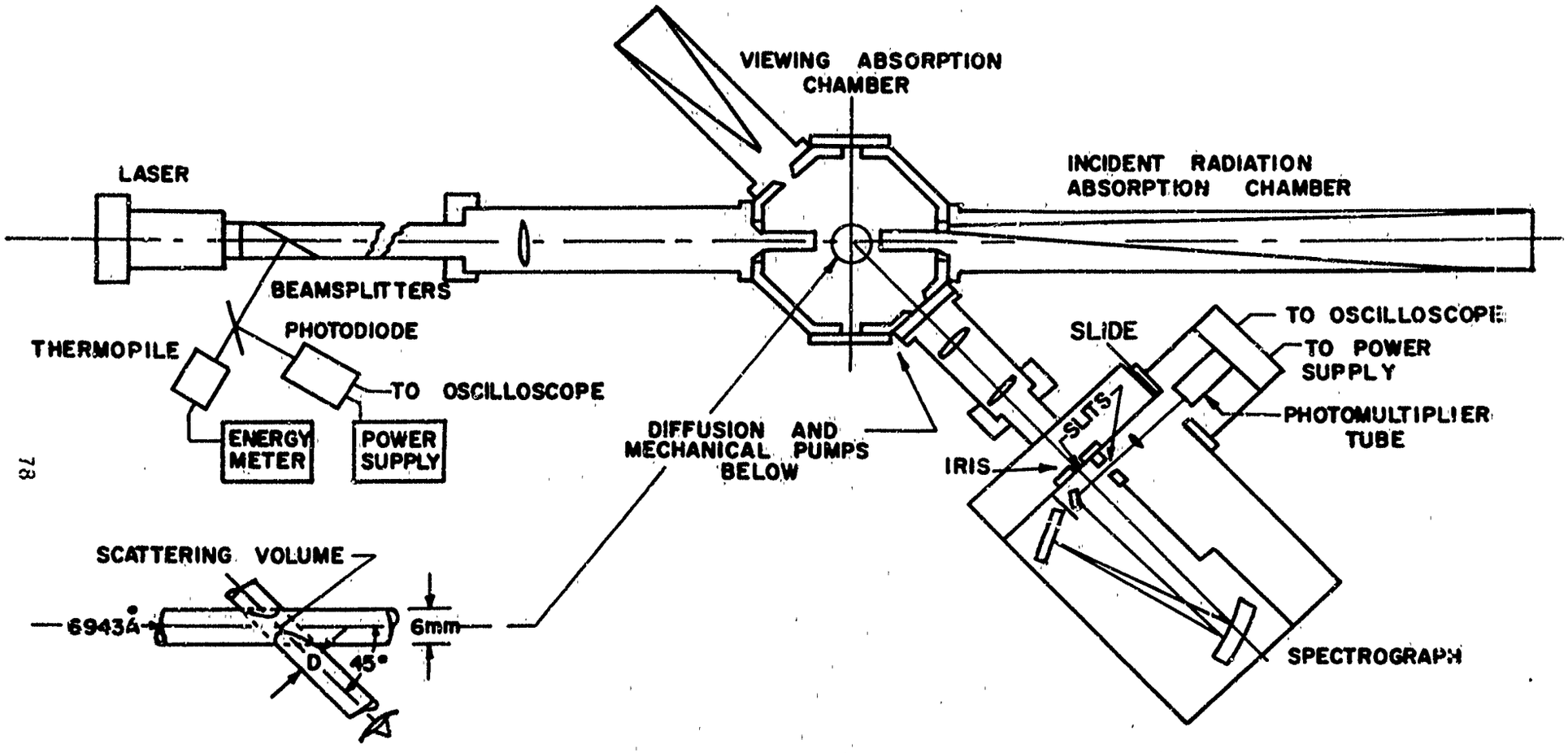

FIG. 6 SCHEMATIC OF THE EXPERIMENTAL APPARATUS

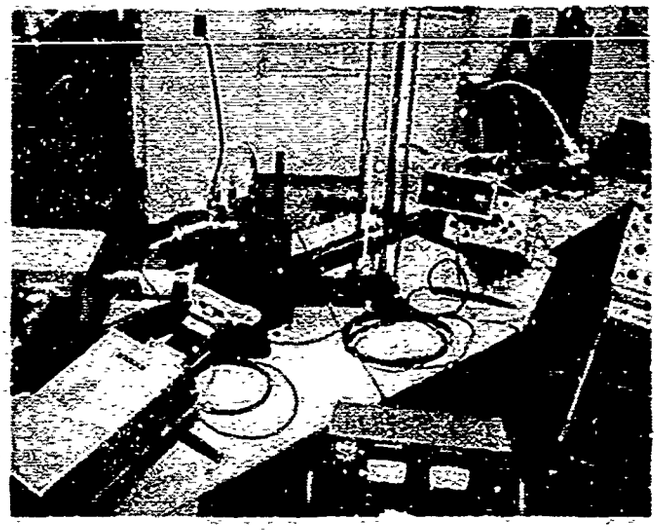

(A) OVERALL VIEW

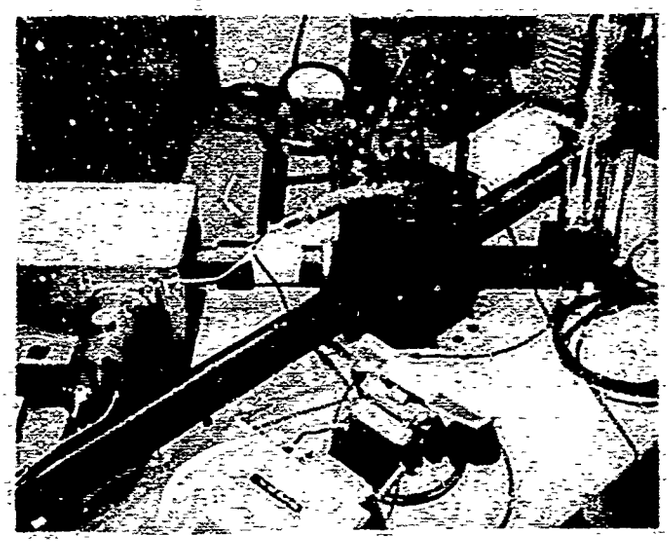

(B) SCATTERING CHAMBER AND SPECTROGRAPH

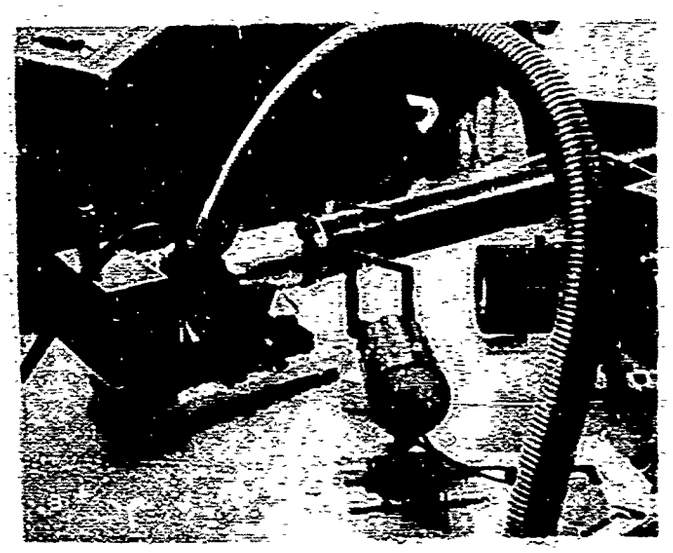

(C) LASER SYSTEM

FIG. 7 PHOTOGRAPHIC VIEWS OF THE EXPERIMENTAL APPARATUS

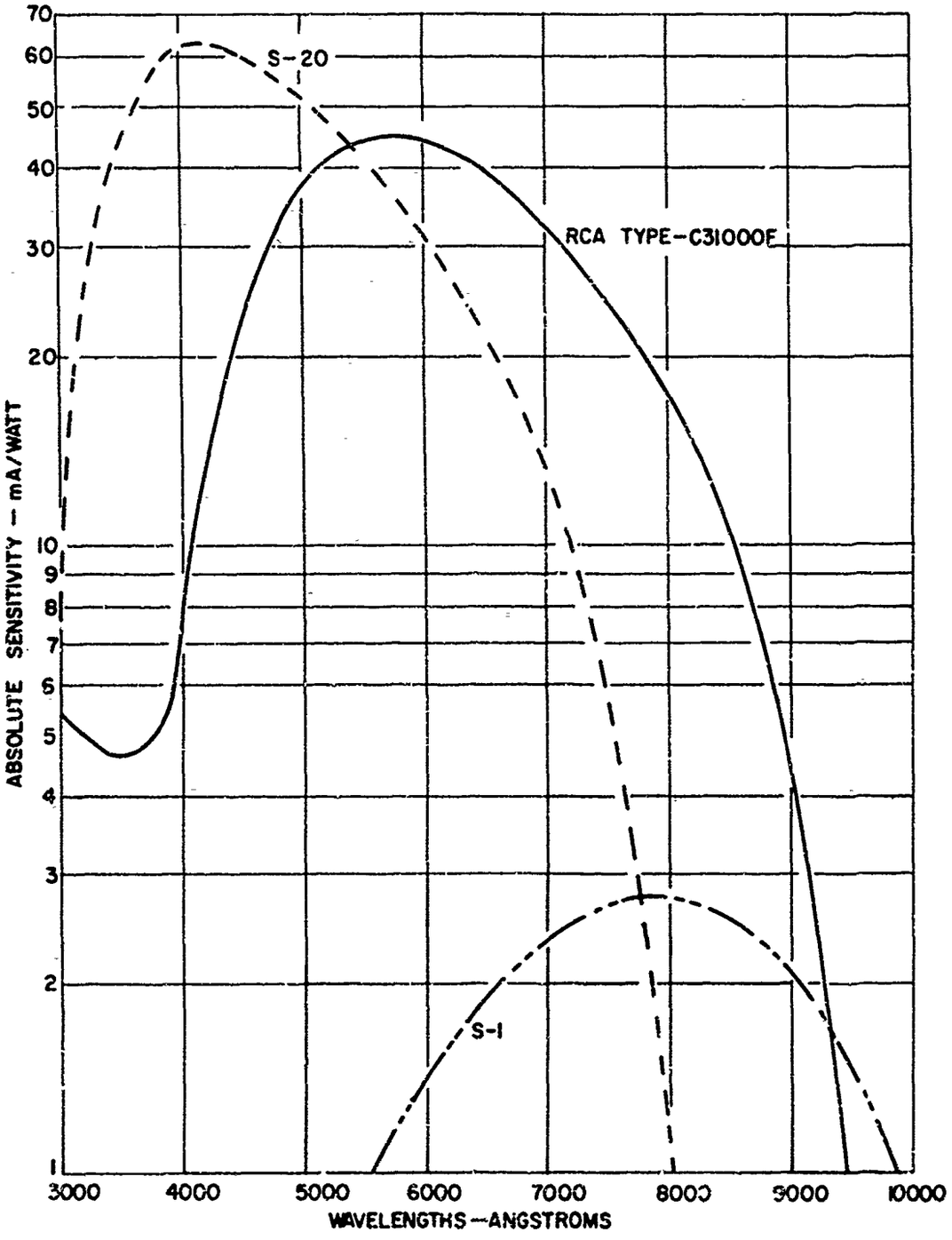

FIG.8 TYPICAL SPECTRAL SENSITIVITIES OF THE PHOTOMULTIPLIER TUBES

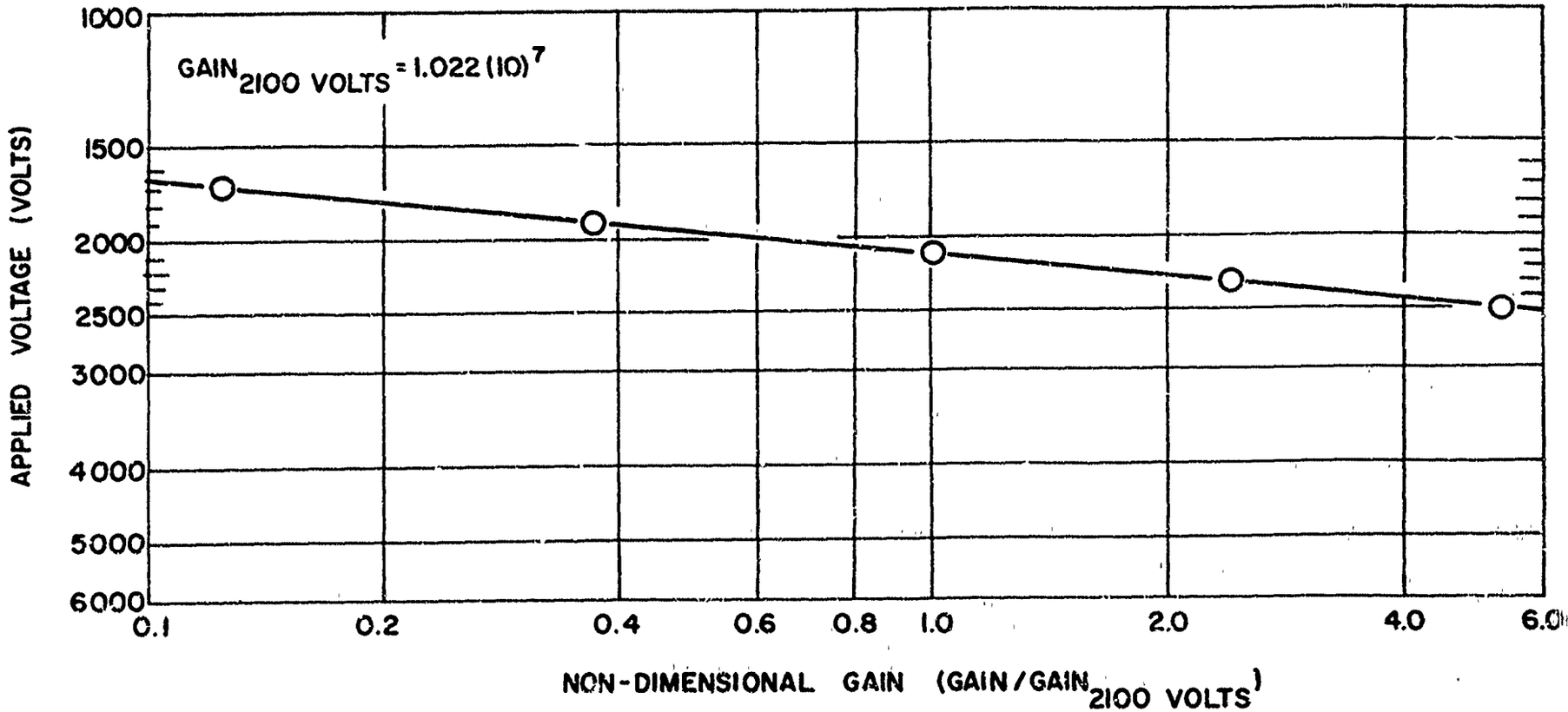

FIG.9 NON-DIMENSIONAL GAIN OF THE PHOTOMULTIPLIER TUBE AS A FUNCTION OF THE VOLTAGE APPLIED BETWEEN THE ANODE AND CATHODE (RCA TYPE-C31000F)

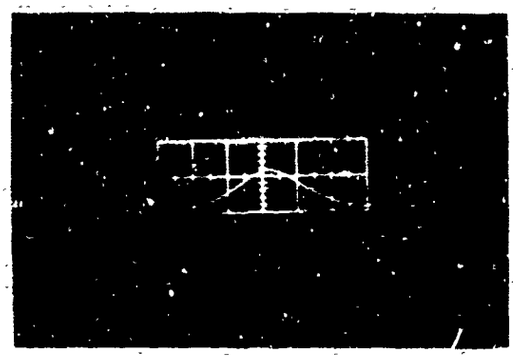

5 NANOSECONDS/DIVISION

(A) LASER PULSE

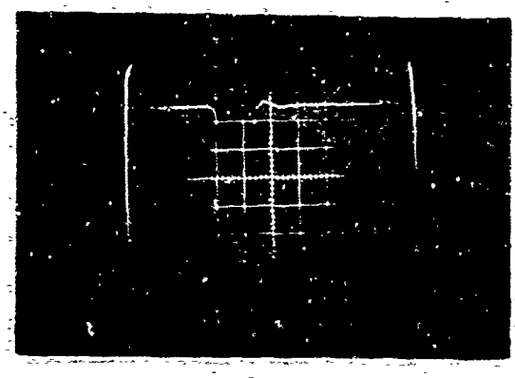

20 NANOSECONDS/DIVISION

(B) RAMAN SCATTERED RADIATION (HIGH PRESSURE)

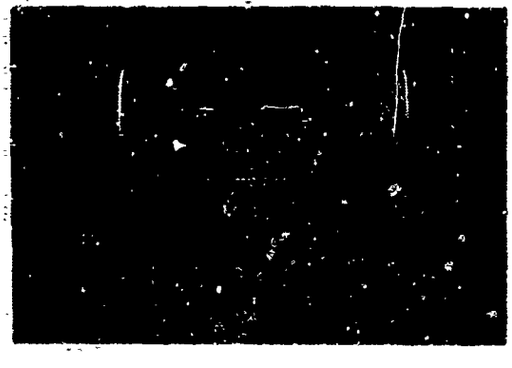

20 NANOSECONDS/DIVISION

(C) RAMAN SCATTERED RADIATION (LOW PRESSURE)

FIG. 10 TYPICAL OSCILLOSCOPE TRACES

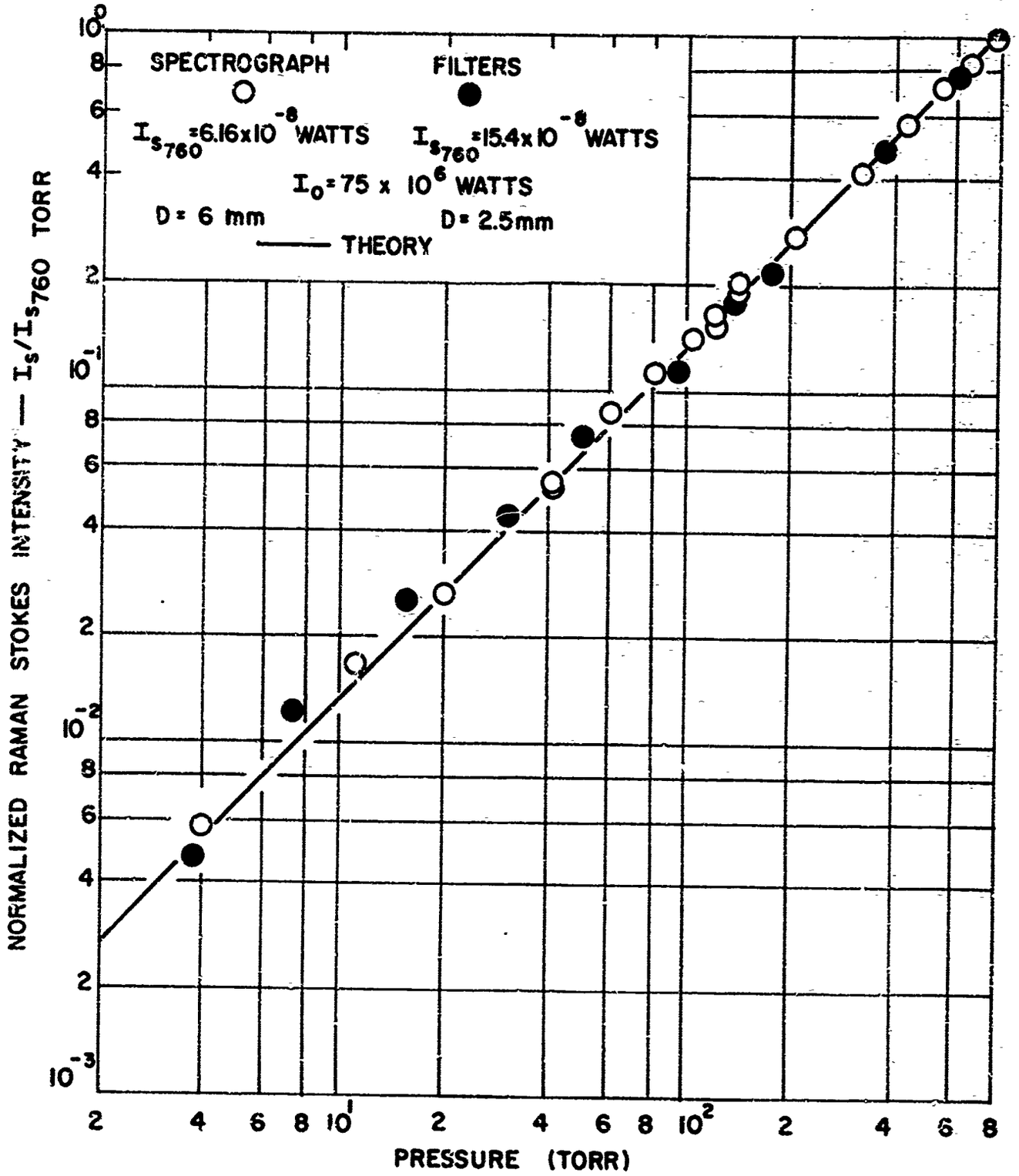

FIG. 12 MEASURED RAMAN STOKES INTENSITY OF OXYGEN (O_2) AS A FUNCTION OF PRESSURE. MEASURED IN AIR AT ROOM TEMPERATURE

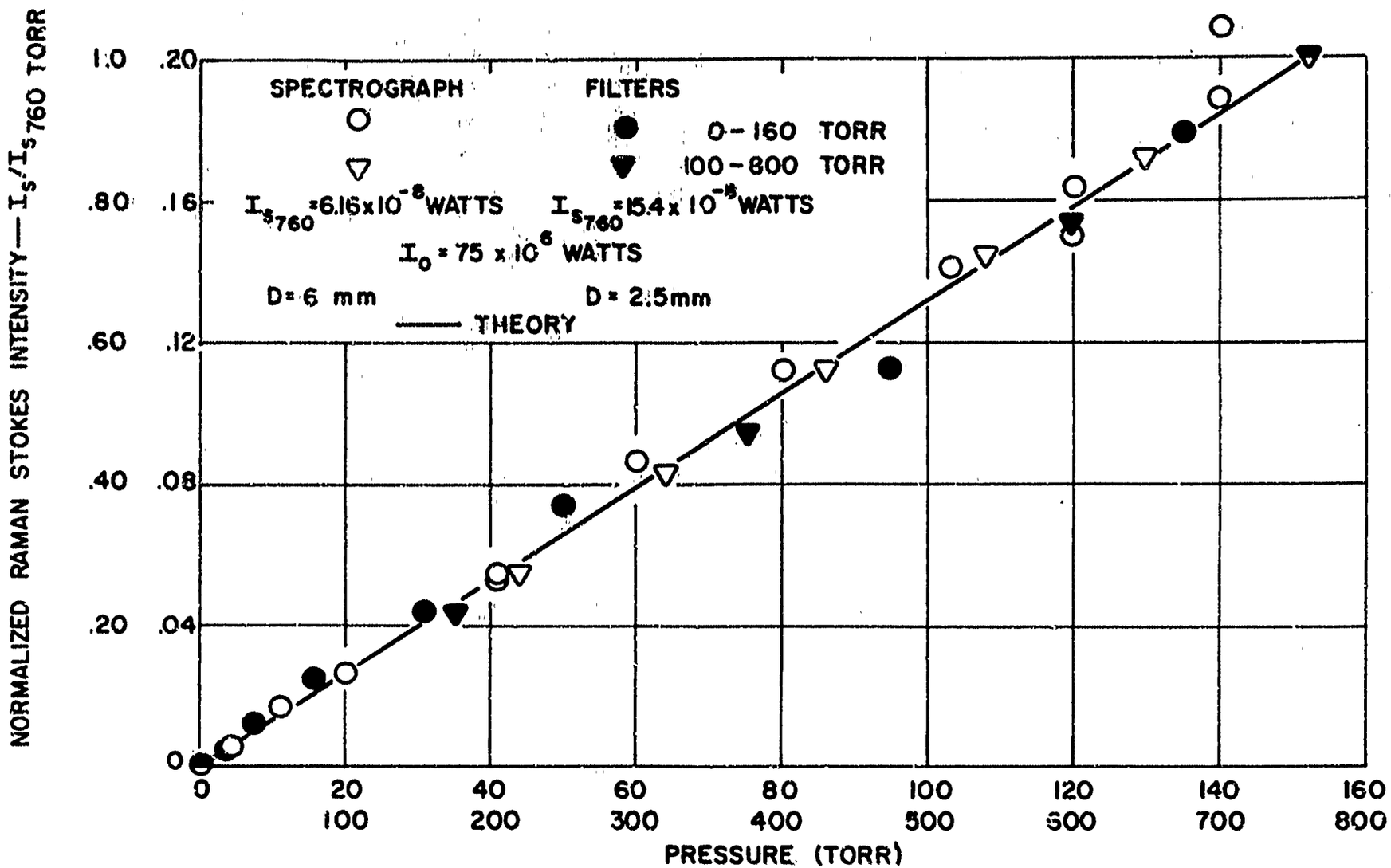

FIG. 11 MEASURED RAMAN STOKES INTENSITY OF OXYGEN (O_2) AS A FUNCTION OF PRESSURE. MEASURED IN AIR AT ROOM TEMPERATURE

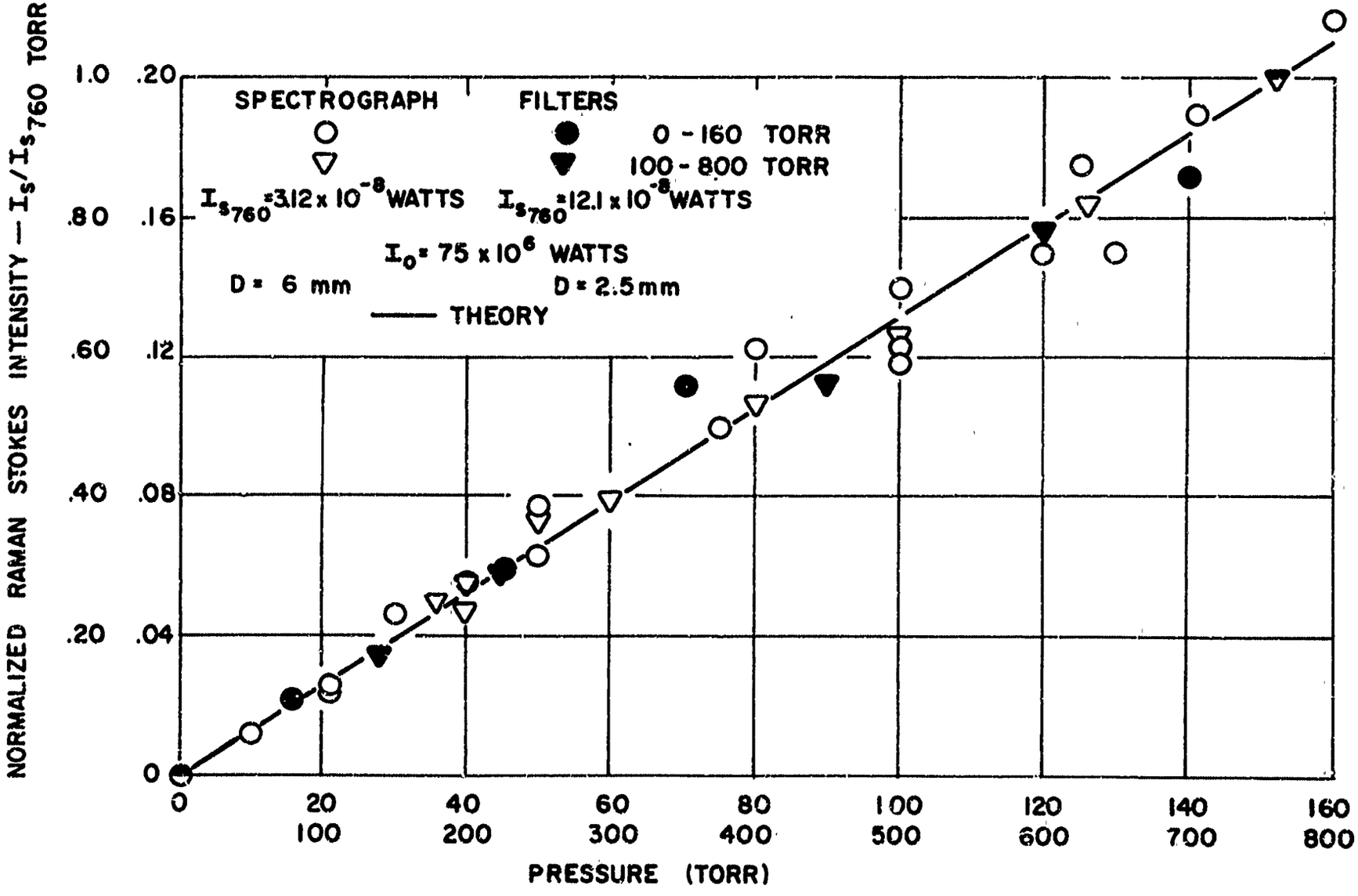

FIG.13 MEASURED RAMAN STOKES INTENSITY OF NITROGEN (N_2) AS A FUNCTION OF PRESSURE. MEASURED IN AIR AT ROOM TEMPERATURE

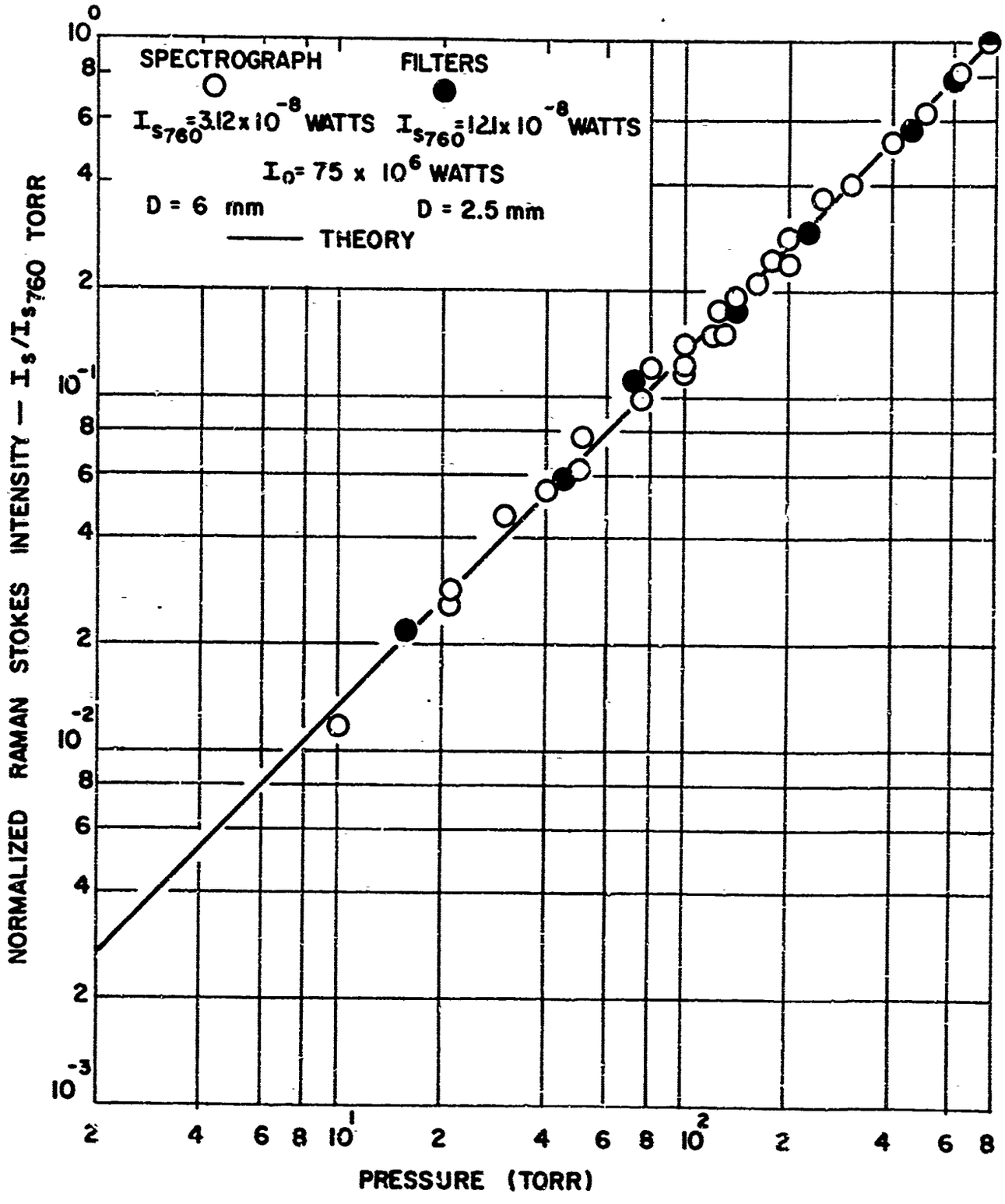

FIG.14 MEASURED RAMAN STOKES INTENSITY OF NITROGEN (N_2) AS A FUNCTION OF PRESSURE. MEASURED IN AIR AT ROOM TEMPERATURE

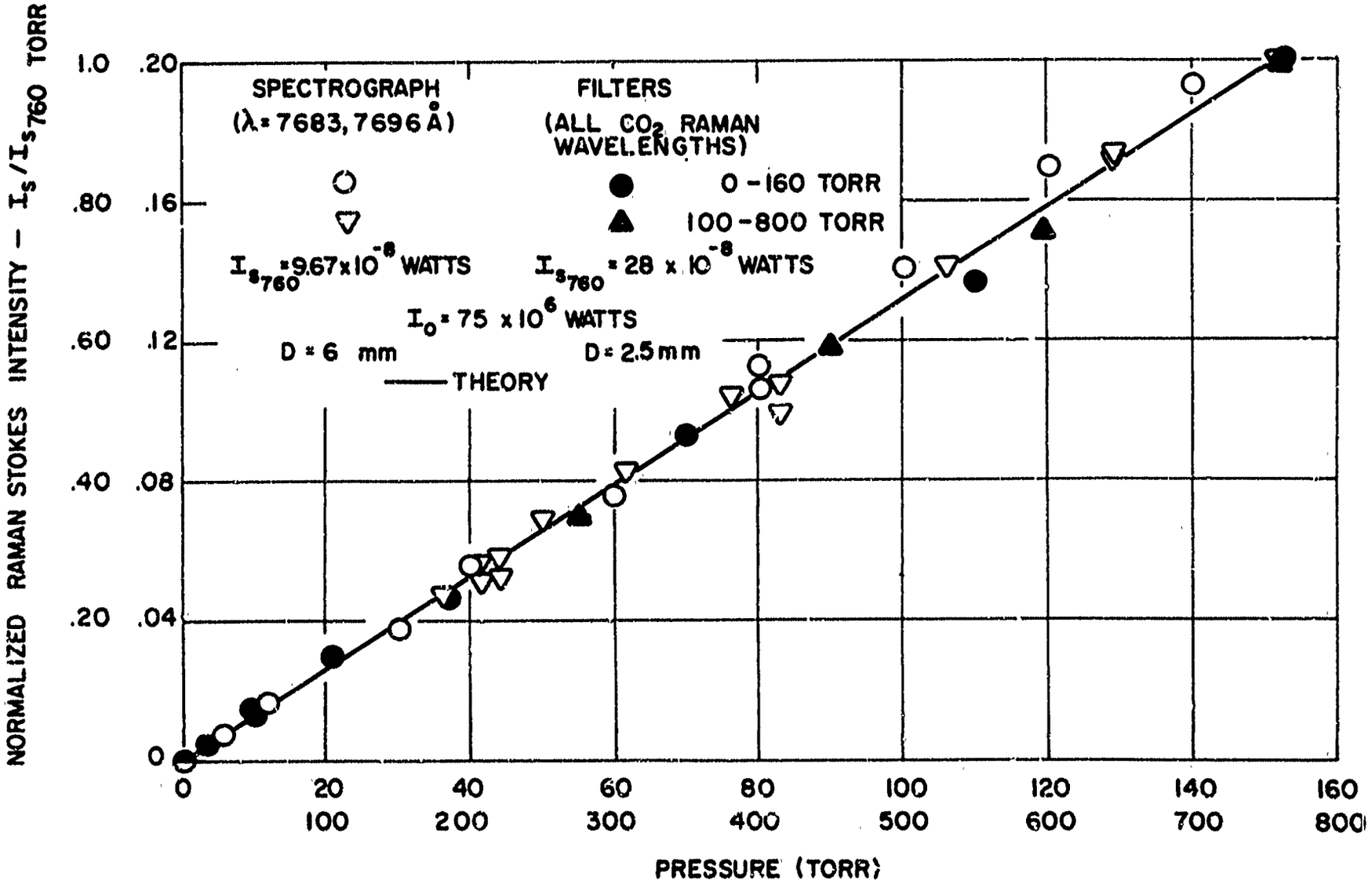

FIG. 15 MEASURED RAMAN STOKES INTENSITY OF CARBON DIOXIDE (CO_2) AS A FUNCTION OF PRESSURE. MEASURED IN AIR AT ROOM TEMPERATURE

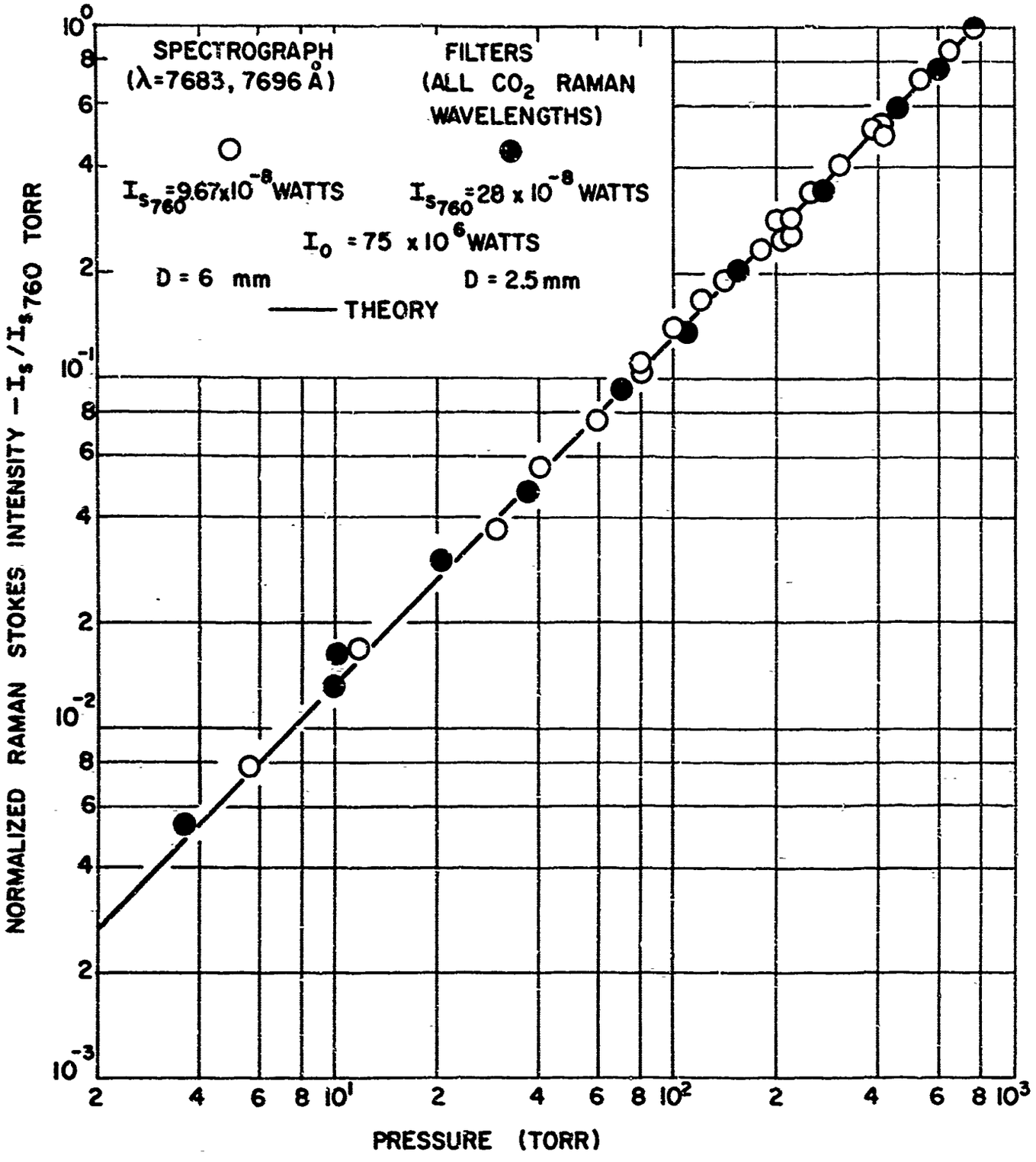

FIG. 16 MEASURED RAMAN STOKES INTENSITY OF CARBON DIOXIDE (CO_2) AS A FUNCTION OF PRESSURE. MEASURED IN AIR AT ROOM TEMPERATURE

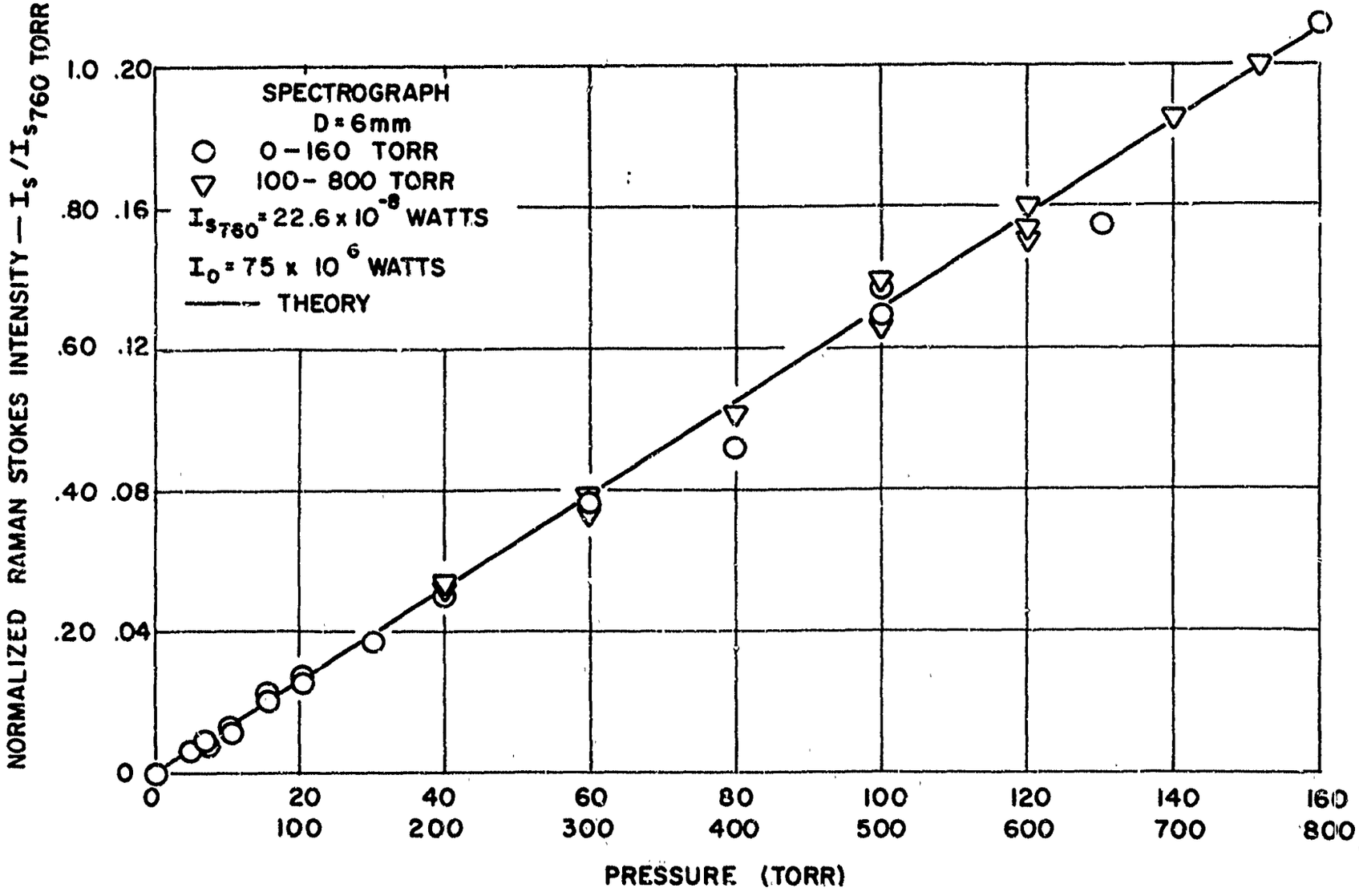

FIG. 17 MEASURED RAMAN STOKES INTENSITY OF METHANE (CH_4) AS A FUNCTION OF PRESSURE. MEASURED IN AIR AT ROOM TEMPERATURE

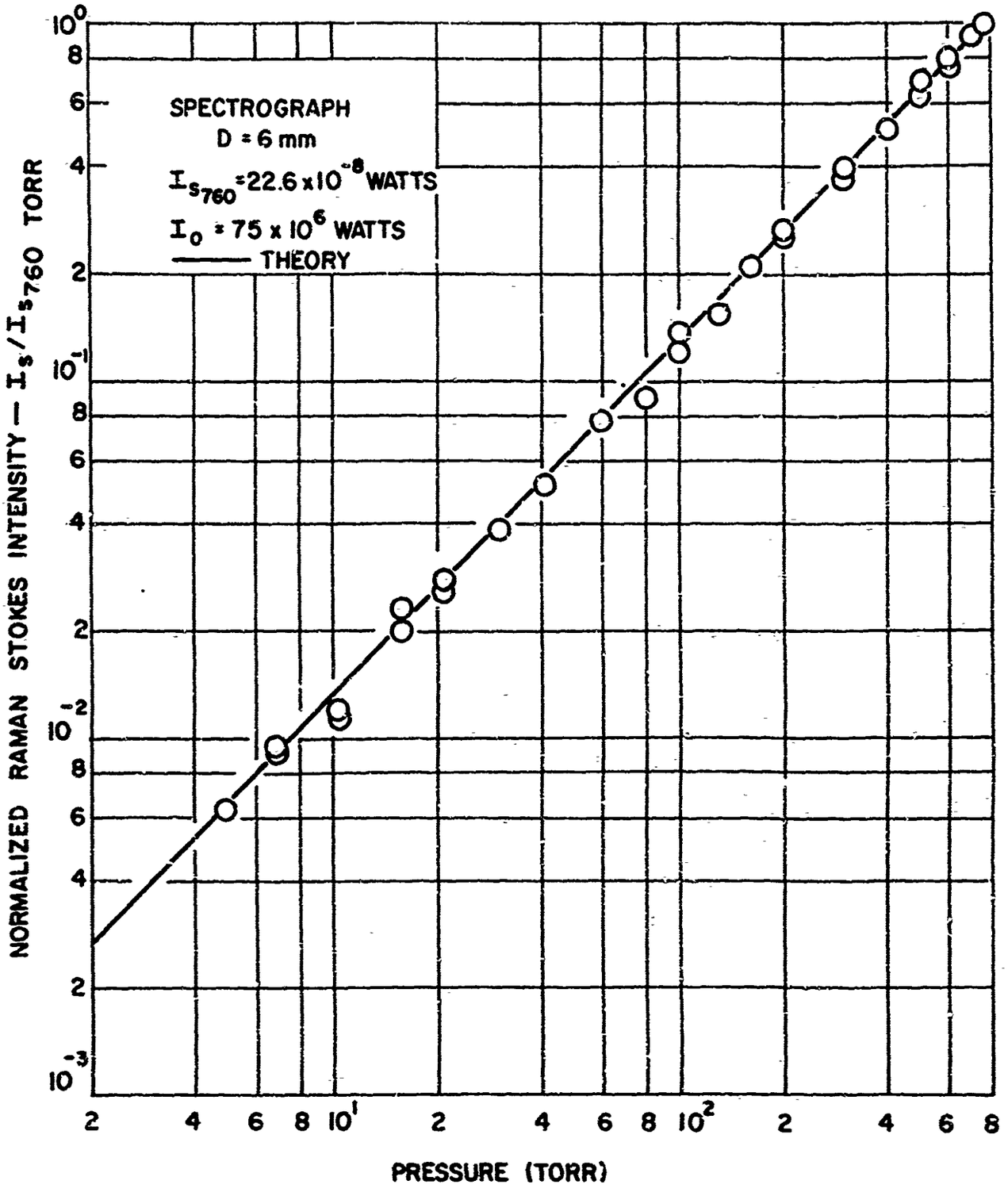

FIG. 18 MEASURED RAMAN STOKES INTENSITY OF METHANE (CH_4) AS A FUNCTION OF PRESSURE. MEASURED IN AIR AT ROOM TEMPERATURE

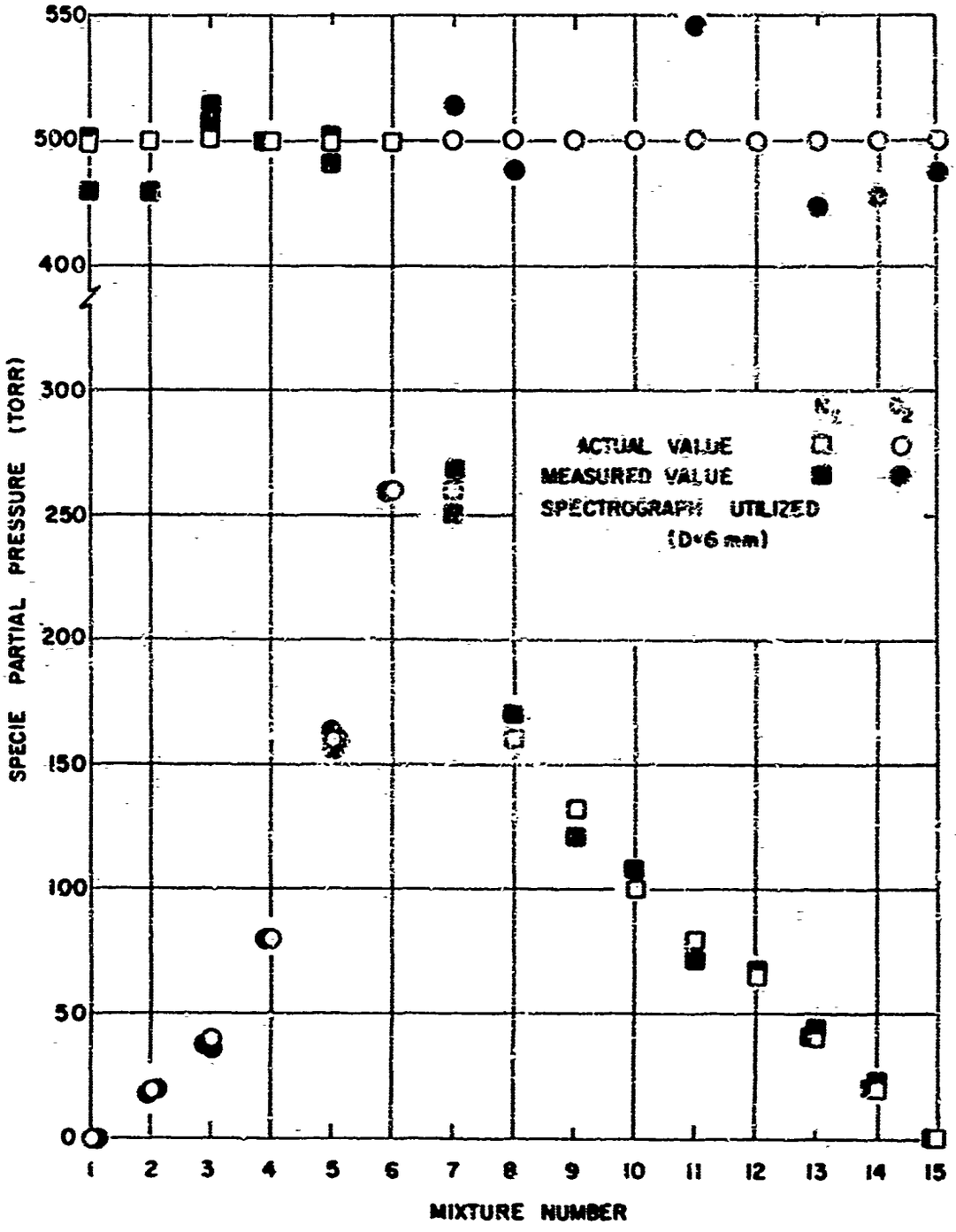

FIG.19 SPECIE CONCENTRATION MEASUREMENTS OF O_2 AND N_2 IN VARIOUS MIXTURE PROPORTIONS USING A SPECTROGRAPH

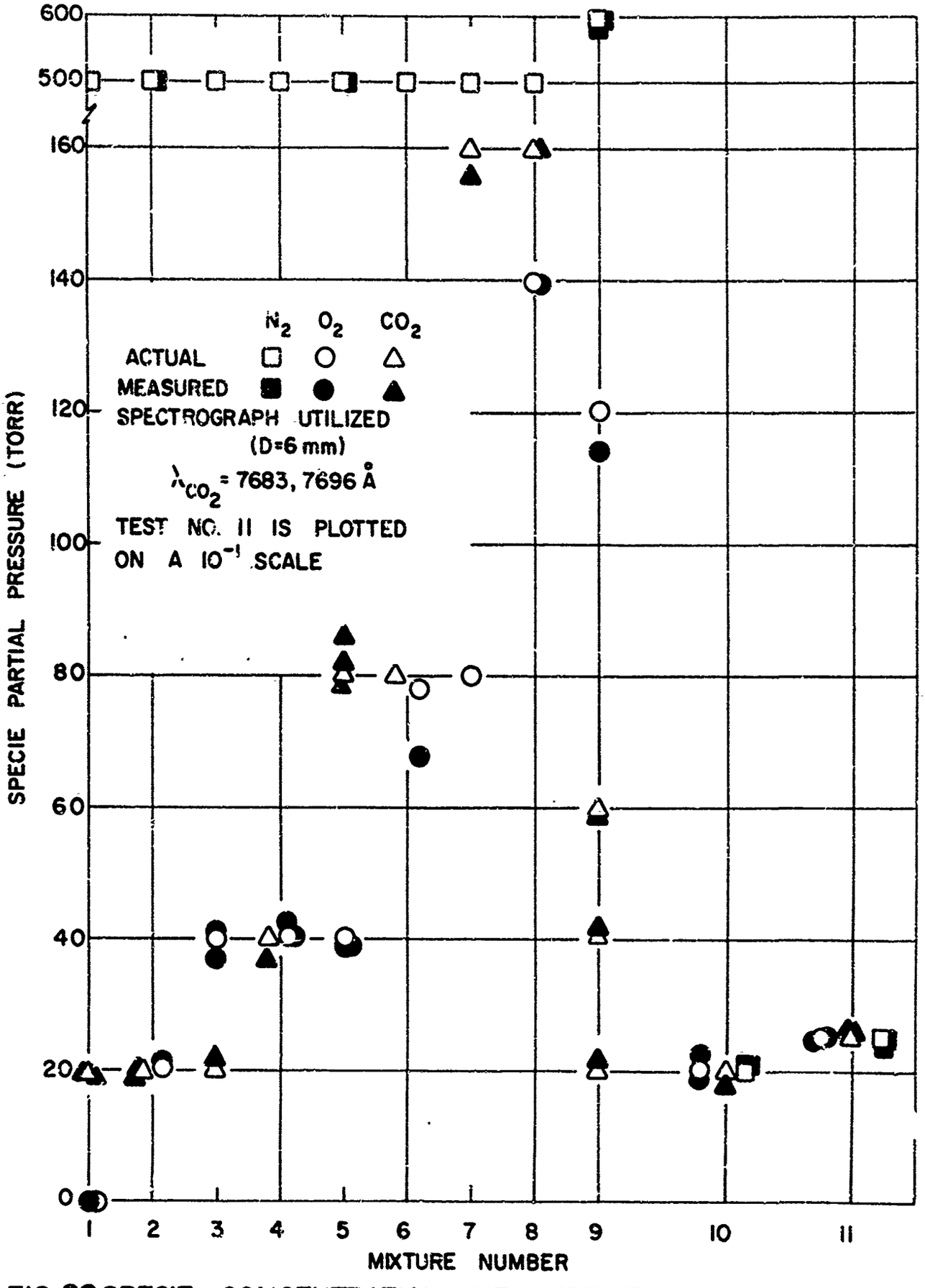

FIG. 20 SPECIE CONCENTRATION MEASUREMENTS OF O_2, N_2, AND CO_2 IN VARIOUS MIXTURE PROPORTIONS USING A SPECTROGRA[illegible]

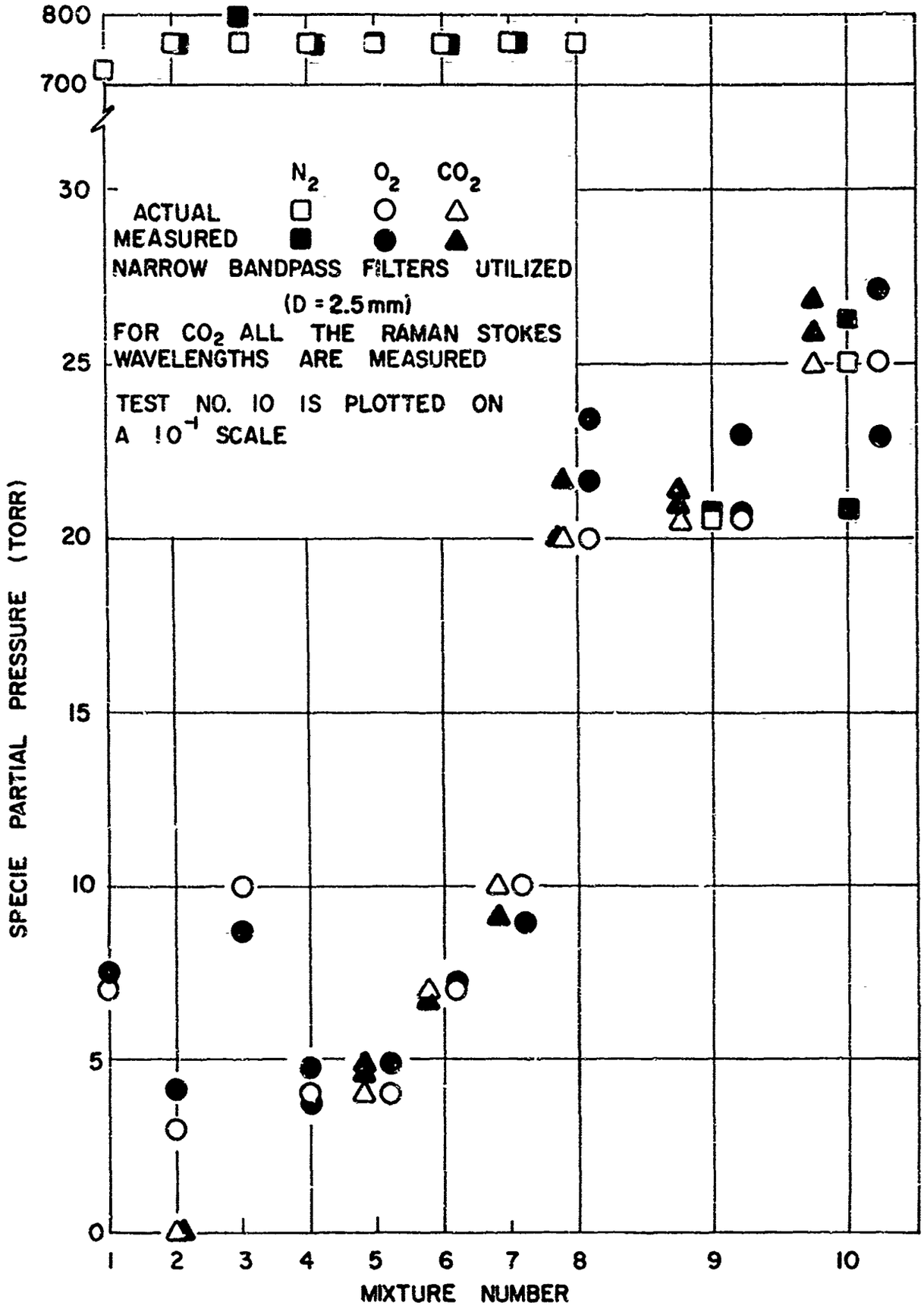

FIG.21 SPECIE CONCENTRATION MEASUREMENTS OF O_2, N_2 AND CO_2 IN VARIOUS MIXTURE PROPORTIONS USING NARROW BANDPASS FILTERS

Unclassified
Security Classification

DOCUMENT CONTROL DATA - R & D

(Security classification of title, body of abstract and indexing annotation must be entered when the overall report is classified)

1. ORIGINATING ACTIVITY (Corporate author)	2a. REPORT SECURITY CLASSIFICATION
Polytechnic Institute of Brooklyn Dept. of Aerospace Engrg. and Applied Mech. Route 110, Farmingdale, New York 11735	Unclassified 2b. GROUP

3. REPORT TITLE

SPECIE CONCENTRATION MEASUREMENTS UTILIZING RAMAN SCATTERING OF A LASER BEAM

4. DESCRIPTIVE NOTES (Type of report and inclusive dates)

Research Report

5. AUTHOR(S) (First name, middle initial, last name)

George F. Widhopf
Samuel Lederman

6. REPORT DATE	7a. TOTAL NO. OF PAGES	7b. NO. OF REFS
November 1969	93	27

8a. CONTRACT OR GRANT NO	9a. ORIGINATOR'S REPORT NUMBER(S)
Nonr 839(38) and DAHCO4-69-C-0077 b. PROJECT NO. ARPA Order No. 529 and c. ARPA Order No. 1442 d.	PIBAL REPORT 69-46 9b. OTHER REPORT NO(S) (Any other numbers that may be assigned this report)

10 DISTRIBUTION STATEMENT

Distribution of this document unlimited

11. SUPPLEMENTARY NOTES	12 SPONSORING MILITARY ACTIVITY
	Office of Naval Research, Washington, D.C. U.S. Army Research Office, Durham, N.C

13. ABSTRACT

The feasibility of utilizing Raman scattering as a diagnostic technique to measure individual specie concentrations in typical gas mixtures found in gas dynamic applications has been investigated and demonstrated. Utilizing this technique, either the local density of a pure gas or the concentration of individual diatomic (or polyatomic) species in a gas mixture can be uniquely determined.

The range and limitations of this technique were investigated and evaluated under controlled static conditions. A Q-switched ruby laser, which has a pulse duration of approximately 10 nanoseconds, was used as a radiation source. The scattered radiation was monitored utilizing a high gain, wide spectral range photomultiplier tube in conjunction with a spectrograph. Measurements were also made utilizing narrow bandpass filters in place of the spectrograph. The species which were investigated include O_2, N_2, CO_2 and CH_4. Quantitative results are given for these gases in their pure state as well as in various mixture proportions.

The relative and absolute intensity of the scattered radiation from the species investigated were compared with that predicted by theory. Good agreement was obtained. Measurements were also made of the vibrational temperature of O_2.

A description of the pertinent theory and concepts of Raman scattering is also included as well as a discussion of the limitations of the technique.

DD FORM 1 NOV 65 1473

Unclassified
Security Classification

14 KEY WORDS	LINK A		LINK B		LINK C	
	ROLE	WT	ROLE	WT	ROLE	WT
Raman scattering						
Rayleigh scattering						
Laser						
Density						
Mixture						
Concentration						
Temperature						
Spectrograph Optical Filters						